Angiopathy with impaired glucose logistics observed in schizophrenia-like model mice

Abbreviated title: Angiopathy in novel schizophrenia-like model mice and patients with schizophrenia

Shinobu Hirai[1,*], Hideki Miwa[1,2], Tomoko Tanaka[1], Kazuya Toriumi[3], Yasuto Kunii[4], Mizuki Hino[4], Ryuta Izumi[4], Atsuko Nagaoka[4], Hirooki Yabe[4], Tomoya Nakamachi[5], Seiji Shioda[6], Takashi Dan[7], Toshio Miyata[7], Yasumasa Nishito[8,] Kazuhiro Suzuki[3], Mitsuhiro Miyashita[3], Masanari Itokawa[3], Makoto Arai[3], Haruo Okado[1,*]

1, Neural Development Project, Department of Brain Development and Neural Regeneration, Tokyo Metropolitan Institute of Medical Science, Tokyo 156-8506, Japan.

2, Molecular Neuropsychopharmacology Section, Department of Neuropsychopharmacology, National Institute of Mental Health, National Center of Neurology and Psychiatry, Tokyo

187-8553, Japan.

3, Schizophrenia Research Project, Department of Psychiatry and Behavioral Sciences, Tokyo Metropolitan Institute of Medical Science, Tokyo 156-8506, Japan.

4, Department of Neuropsychiatry, School of Medicine, Fukushima Medical University, Fukushima 960-1295, Japan.

5, Laboratory of Regulatory Biology, Graduate School of Science and, Engineering, University of Toyama, Toyama 930-8555, Japan.

6, Global Research Center for Innovative Life Science, Peptide Drug Innovation, Hoshi University, Tokyo 142-8501, Japan.

7, Division of Molecular Medicine and Therapy, Tohoku University Graduate School of Medicine, Miyagi 980-8575, Japan.

8, Center for Basic Technology Research, Tokyo Metropolitan Institute of Medical Science, Tokyo 156-8506, Japan.

*These authors contributed equally to this work.

Correspondence should be addressed to Shinobu Hirai and Haruo Okado, Neural Development Project, Department of Brain Development and Neural Regeneration, Tokyo Metropolitan

Institute of Medical Science, Tokyo 156-8506, Japan. E-mail: hirai-sn@igakuken.or.jp (S.H.) and okado-hr@igakuken.or.jp (H.O.)

Number of figures: 6

Number of tables: 0

Number of supplementary figures: 5

Number of supplementary tables: 3

Key Words: schizophrenia, angiopathy, glucose metabolism, sugar intake, animal models, Parvalbumin-positive interneurons

Author contributions

S.H. and H.O. designed research. S.H. performed and analyzed all experiments. H.M. helped with experimental design of EEG recording and analysis of the results, and edited the manuscript. T.T. coordinated the EEG recording. Y.K., M.H., R.I., A.N., and and H.Y. helped with design of experiment using human specimens and provided the sections of fixed human

brains. T.N. and S.S. provided GFAP-GFP mice. T.D. and T.M. generated and provided *Glo1* knockout (KO) mouse. K.T. and K.S. backcrossed *Glo1* KO mice to B6J mice for all experiments. M.I., M.A., K.T., K.S. and M.M. helped this study with important suggestions. S.H. generated all figures, tables, and wrote the manuscript. H.O. edited the manuscript and supervised this study.

Acknowledgments

We would like to thank MS. Sayaka Ogikubo, MS, Yoshie Matsumoto, MS. Haimei Zhang and MS. Minami Murata, Izumi Nohara, Yukiko Shimada, Emiko Hama, Nanako Obata, Mai Hatakenaka, Chikako Ishida for their contribution to help us with experiments related to this research. We also thank Dr. Tohru Kodama for teaching us about microdialysis and encephalogram recording, Dr. Jun Horiuchi and Dr. Kenji Tanaka for review the study, Ms. Chiaki Watanabe and Ms. Hiromi Onuma for their contribution to coordinating donations of postmortem brains, Prof. Hideki Chiba for the preparation of postmortem brain samples. We also express our gratitude to the families of the deceased for the donations of brain tissue and

their time and effort devoted to the consent process and interviews. This work was supported by Japan Society for the Promotion of Science KAKENHI Grant 18K14832 (to S.H.), 17K18395, 19K08033 (to H.M.), 17K16408 (to T.T.), 18H02537, 18K19383 (to H.O.) and also by the Ichiro Kanehara Foundation, the Japan Prize Foundation and the Takeda Science Foundation (to S.H.), Strategic Research Program for Brain Sciences from AMED Grant JP19dm0107107 (to H.Y.), and Grant-in-Aid for Scientific Research on Innovative Areas from the MEXT JP16H06277 (to H.Y.). This research was also supported by KAKENHI Grant Numbers: 16H05380（to M.A.）, 18K06977（to K.T.）19H03589（to M.I.）, 18K15354（to K.S.）, AMED Grant Number: JP19dm0107088（to M.I.）, The Kanae Foundation for the Promotion of Medical Science（to K.T.）and The Uehara Memorial Foundation（to M.A.）.

ABSTRACT

Dietary sugar in humans has increased dramatically in the modern era. However, it is unclear whether and how high sugar diets affect the pathogenesis of psychiatric disorders. Here we demonstrate that a high sugar diet induces expression of schizophrenia-associated positive, negative, and cognitive symptoms in mice deficient for glyoxalase-1, an enzyme associated with schizophrenia involved in the detoxification of carbonyl compounds. We found that a high sugar diet increased nondiabetic vascular damage in glyoxalase-1 mutant mice, and reduced glucose uptake into the brain parenchyma. Chronic aspirin treatment reduced vascular damage, increased glucose uptake into the brain, and prevented development of several schizophrenia-associated phenotypes. Postmortem analysis of brains from patients with schizophrenia revealed similar vascular damage to what we observe in our mutant mice. Our results indicate that schizophrenia is associated with vascular damage likely caused by metabolic dysfunction.

In response to a global increase in free-sugar intake, in 2015, the World Health Organization

(WHO) published guidelines that addressed concerns about the impact of sugar intake on body weight gain and the development of dental caries[1]. Body weight gain or high sugar intake itself increase the risk of a variety of chronic diseases, including diabetes, hypertension, and kidney disease[2-5]. However, the effect of high sugar intake on mental health, and on schizophrenia more specifically, has not been investigated thoroughly. Schizophrenia is a multifactorial disease that develops through complex interactions between multiple genes and environmental risk factors[6]. In recent years, "urbanity" has been considered a new environmental risk factor for schizophrenia; within this concept, low social cohesion is indicated as a novel risk factor for this disease[7,8]. Thus, it is important to reconsider environmental factors in the understanding of the etiology and pathogenesis of schizophrenia, because of the modernization of diets and living environments.

A large body of research indicates the presence of an increased level of oxidative stress in patients with schizophrenia[9-11]. Oxidative stress facilitates the formation of advanced glycation end products (AGEs), which are generated by non-enzymatic reactions between some sugars or reactive carbonyl compounds and the amino group of large biomolecules, including proteins, nucleic acids, and lipids; in addition, they may induce inflammatory reactions, through their

receptor (receptor of AGEs, RAGE), for example[12]. As reactive carbonyl compounds are among the major sources of AGEs, oxidative stress is also called "carbonyl stress." [13] About 20% of patients with schizophrenia exhibit increased blood levels of pentosidine, which is a type of AGE, and decreased levels of vitamin B6[14,15], implying that a high level of carbonyl stress exists in many of these patients. The glyoxalase I (*GLO1*) gene encodes a zinc metalloenzyme that protects cells from AGE toxicity by reducing the levels of reactive carbonyl compounds[16]. In a patient with schizophrenia who exhibited poor convalescence, a frameshift mutation in *GLO1* has been reported, which was accompanied by reduced activity of the GLO1 enzyme[15,17]. A trend toward elevated AGE accumulation in plasma and reduced GLO1 activity has been observed in patients with schizophrenia compared with control subjects[14]. Therefore, we hypothesized that GLO1 plays an important role in schizophrenia by removing the excess of carbonyl compounds induced by high sugar intake.

Interestingly, patients with schizophrenia consume 1.5 times as much sugar as do healthy individuals[18]; moreover, patients who consume more sucrose exhibit a worse 2-years outcome[19]. However, whether excessive sugar consumption is a cause of schizophrenia or merely an abnormal behavior of these patients during the disease process remains unknown. Taking the

functions of GLO1 into account, we hypothesized that excessive sugar intake is strongly associated with the pathogenesis of schizophrenia under matched genetic circumstances. Here we propose that excessive sugar consumption during adolescence is a potential environmental risk factor for schizophrenia. We addressed this hypothesis by generating a mouse model based on the gene–environment interaction approach and identified a novel phenotype of schizophrenia, "angiopathy," both in our mouse model and in patients with schizophrenia, and the model mice particularly showed an abnormal glucose logistics.

Results

Behaviors of *Glo1* heterozygous mice on a high-sucrose diet

To prove our hypothesis that excessive sugar intake during adolescence is an environmental risk factor for schizophrenia, we prepared two diets containing the same caloric percentages of carbohydrates, fat, and proteins (**Fig. 1a, and see the Methods section**). We investigated four groups of mice that were fed these diets for about 50 days immediately after weaning (from postnatal day 21): wild-type, starch-fed mice (control, CTL); wild-type, sucrose-fed mice

(environmental stressor, Env); *Glo1* heterozygous, starch-fed mice (genetic factor, Gen); and *Glo1* heterozygous, sucrose-fed mice (combination of the genetic factor and the environmental stressor, G×E) (**Fig. 1a**). This 50-day period in mice corresponds to human adolescence, during which schizophrenia often first appears[20]. Western blot analysis revealed that *Glo1* heterozygous mice exhibited reduced GLO1 expression levels in their cerebral cortices, including the hippocampus (**Supplementary Fig. 1a,b**); moreover, their body weight trajectories were similar to those of the control mice up to 11 weeks of age, which was indicative of a normal structural development (**Supplementary Fig. 1c**). We did not observe any significant differences between CTL, Env, and Gen mice regarding locomotor activity (**Fig. 1b**), pre-pulse inhibition (PPI; used for estimating the sensory motor gating ability) (**Fig. 1d**), and object-location tests (used for quantifying working memory) (**Fig. 1e**). Note that only G×E mice showed increased locomotor activity, decreased PPI scores, and working memory deficits compared with CTL mice (**Fig. 1b,d,e**). A decline in acoustic startle responses was observed in *Glo1* heterozygous mice, regardless of diet (**Fig. 1c**). Effects of the environmental factor, but not of the genetic one, were observed in the self-grooming test, the nest-building test, and the elevated plus-maze test (**Fig. 1f,g, and Supplementary Fig. 2a**). No differences were detected in the social interaction test

among the four groups (**Supplementary Fig. 2b**). These behavioral abnormalities of *Glo1* heterozygous mice on a high-sucrose diet (G×E mice) are considered to reflect schizophrenic symptoms consisting of positive symptoms (**Fig. 1b**), negative symptoms (**Fig. 1g**), and cognitive deficits (**Fig. 1d, e**)[21]. In addition, excessive sucrose intake itself triggered several abnormal behaviors, regardless of genotype (**Fig. 1f, g, and Supplementary Fig. 2a**).

Increased dopamine (DA) release at the basal level and an amphetamine-induced condition in the striatum, including the nucleus accumbens (NAc), are characteristic of schizophrenia[22,23]. This dopamine increase in the NAc causes hyper-locomotion in mice[24], whereas DA depletion in the NAc suppresses amphetamine-induced hyperactivity[25,26]. Therefore, we measured DA release in the NAc of our model mice using *in vivo* microdialysis and found that G×E mice alone exhibited an elevated basal release of DA and an abnormally enhanced reactivity to methamphetamine injection in the NAc (**Fig. 1h**). Next, to confirm whether the therapeutic agent used in patients with schizophrenia was as effective in our model mice, aripiprazole (0.5 mg/kg/day) was administered to G×E mice during the last 7 days of sucrose feeding (**Fig. 1a,i–k, and Supplementary Fig. 2c–f**). The main efficacies of aripiprazole are attributed to partial agonism of dopamine D2 receptors (D2Rs)[27] and this drug is generally used in schizophrenia as

the first-choice antipsychotic agent. The hyper-locomotion activity and increased DA release in the NAc observed in G×E mice were completely restored by aripiprazole treatment (**Fig. 1h, i**), indicating that the observed elevated locomotion activity was caused by increased DA release. Moreover, the reduced PPI and working memory deficits were partially improved by the administration of aripiprazole (**Fig. 1j, k**). Conversely, the results of the self-grooming, elevated plus-maze, and nest-building tests were not improved by aripiprazole treatment (**Supplementary Fig.2 d–f**). In summary, aripiprazole treatment yielded a great improvement of positive-like symptoms and a mild improvement of cognitive defects in our mouse model of psychiatric disease. These results are in accordance with those of a previous case report that found that the antipsychotic drugs used currently are efficacious for positive symptoms but, with few exceptions, lack efficacy for negative, and cognitive symptoms[28,29]. Thus, our G×E model mice have a good predictive validity, as they provide an indication regarding the effectiveness of antipsychotic drugs.

Dysfunction of parvalbumin-positive inhibitory interneurons in G×E mice

Normal parvalbumin (PV)-positive GABAergic neuron activity is crucial for the maintenance of

normal PPI and working memory; moreover, PV neuron hypo-function induces hypersensitivity to dopamine neurons in the presence of psycho-stimulants, such as amphetamine[30-33]. A decreased number of PV neurons has been repeatedly reported in studies of postmortem brains of patients with schizophrenia[34-36] and in animal research[32,37]. Thus, we examined the expression levels of PV using immunohistochemistry and Western blotting. The number of PV-positive cells was clearly lower in the hippocampus of sucrose-fed mice compared with the starch-fed mouse group and the CTL group (**Fig. 2a, b**). The intensity of the PV signal in the hippocampus was also decreased in G×E mice (**Fig. 2c, d**). To clarify whether this downregulation of PV was accompanied by functional abnormalities, gamma oscillation (30–45 Hz) was measured using surface electroencephalography (EEG). Gamma oscillations are produced by synchronous activation of PV neurons[38,39] and an increase in gamma oscillation power is observed during a variety of perception and cognition tasks in the visual cortex and prefrontal cortex in animals[40,41] and humans[42-44]; in contrast, this parameter is disturbed in schizophrenic patients[45]. With this property in mind, we evaluated PV neuronal function in our model; G×E mice alone did not exhibit an increase in the gamma oscillation power when they approached the novel object (**Fig. 2e, f**). Interestingly, sucrose-fed mice showed an elevated baseline gamma

oscillation power compared with starch-fed mice in the home cage (**Fig. 2e**). These results are consistent with the findings of a study of patients with schizophrenia and of studies of other schizophrenia model mice, i.e., increased baseline gamma oscillations and decreased sensory-stimulus-evoked gamma power[33,46,47]. Therefore, our results suggest that G×E mice mimic the pathophysiological changes of PV neurons observed in schizophrenia.

To summarize these results, the administration of a high-sucrose diet to *Glo1* heterozygous mice causes schizophrenia-like psychiatric conditions at the behavioral, histological, pathophysiological, and pharmacological levels, which suggest that excessive sucrose intake during adolescence is a potential environmental risk factor for schizophrenia.

AGE accumulation and impaired astrocyte function in G×E mice

Next, to investigate the mechanisms underlying the emergence of these psychiatric phenotypes, especially in G×E mice, we first assessed the GLO1 expression patterns. The strongest GLO1 expression was detected in astrocytes, especially in those that surrounded capillaries (**Supplementary Fig. 3a–f**). In contrast, we observed moderate GLO1 expression in neurons and weak GLO1 expression in microglia and vascular endothelial cells, which appeared to be

sparsely localized (**Supplementary Fig. 3g–i**), and the expression of this protein was not detected in *Glo1* homozygous mice (**Supplementary Fig. 3m**). Considering the function of the GLO1 protein, an enhanced AGE production is expected in G×E mice. Immunohistochemistry aimed at assessing these compounds showed a clear and strong fluorescent AGE-immunoreactive signal, which was detected using an ab23722 antibody, in the vascular endothelial cells of G×E mice compared with CTL mice (**Fig. 3a–g**). We also detected another AGE (AGE-4), which is a product of fructose and carbonyl compounds metabolism, in the microglia of sucrose-fed mice, which was accompanied by changes in microglial ramification properties (**Supplementary Fig. 4a,e**). Microglia in sucrose-fed groups exhibited a greater number of processes compared with the starch-fed groups (**Supplementary Fig. 4a,e**). Microglial morphological responses to pathophysiology are diverse, ranging from hyper-ramified to amoeboid shapes and hyper-ramified morphologies were previously identified in mice with chronic stress[48,49]. In general, cellular damage is caused by the activation of inflammatory responses via the RAGE or by altered protein function that deprive proteins of their original function of proteins by AGE forming reactions[50]. While these processes may alter various signaling pathways in AGE-accumulating cells and their surrounding cells[51], it is not

possible to investigate the expression patterns of all AGEs. Because we detected strong GLO1 expression in astrocytes (**Supplementary Fig. 3a–f**), we used transgenic mice in which the level of green fluorescent protein (GFP) expression can be upregulated under the control of the glial fibrillary acidic protein (*GFAP*) gene promoter in response to the activation of astrocytes[52,53]. Strongly enhanced *GFAP* promoter function was observed in G×E mice, without changes in the number of GFAP-positive astrocytes (**Fig. 3h–j**); this indicates that the astrocytes in G×E mice are in the reactive astrocyte pre-condition, in which GFAP is intensively expressed[54,55]. Taken together, AGE accumulation occurs in cells with low GLO1 expression (**Fig 3a–g and Supplementary Fig. 3, 4**) and astrocytes are activated by a high-sucrose diet combined with GLO1 downregulation and exhibit a pre-inflammatory status (**Fig 3h–j**), which is consistent with the condition of schizophrenic brains[56].

Vascular injury and impaired glucose intake in G×E mice

To understand the processes of G × E mouse brains, we conducted a transcriptome analysis of PFC regions using microarray experiments among the four groups of mice (**Fig. 4a, b**). The coagulation factor V, which is an essential participant in the processes of production of fibrin

from fibrinogen, ranked seventh on the list of transcripts that exhibited more than doubled expression levels in G×E mice compared with the remaining three groups (**Fig. 4a, Supplementary Table 1, 2**). We then attempted to investigate the functional conditions of the endothelial cells via immunohistochemistry using anti-fibrin antibodies, as fibrin plays a role in hemostasis via polymerization with platelets, to form blood clots, and deposits of this protein are indicative of tissue injury, regardless of the nature of the inciting event, including injuries driven by mechanical insult, infection, or immunological derangements[57]. For example, in the early stage of impairment of endothelial cells, fibrin accumulates in capillaries, unlike the deposition of fibrin that is observed in the brain parenchyma of patients with Alzheimer disease[58-60]. We confirmed the presence of a significant fibrin accumulation in the vascular lumen side of endothelial cells in the brain capillaries of G×E mice (**Fig. 4c–f**).

Next, we hypothesized that the damaged vascular endothelial cells observed in the G×E mice affect the uptake of glucose from the plasma into the brain parenchyma. We measured the extracellular concentrations of glucose in the brain parenchyma at three time points: 1) in the fasting condition; 2) 1 h after eating; and 3) 2 h after eating. Contrary to our expectations, we detected a significant impairment of glucose intake into the brain parenchyma 1 h after eating in

the G×E mice (**Fig. 4g**). No differences were observed in plasma glucose and fasting plasma insulin levels among the four groups (**Fig. 4h, i**), which indicates that impaired glucose uptake is independent of the regulation of plasma glucose and insulin levels.

Protective effects of chronic low-dose aspirin treatment regarding behavior and angiopathy

Previous reports showed that interventions with an adjunctive use of NSAIDs improve the scores of patients with schizophrenia on the Positive and Negative Syndrome Scale compared with placebos[61,62]. Aspirin, a type of NSAID, is regularly used for the prevention and alleviation of vascular-related events, such as high blood pressure, ischemia, and cardiovascular diseases[63-67]. Thus, we examined whether aspirin treatment has protective effects against the development of abnormal behaviors in G×E mice (**Fig. 1a, Fig. 5a–d and Supplementary Fig. 5a–c**). The administration of aspirin at a low dose (1 mg/kg/day) led to the effective prevention of deficits in working memory and grooming duration in G×E mice (**Fig. 5c and Supplementary Fig. 5b**) and ameliorated partially the hyper-locomotor activity, PPI deficits, nest-building skills and the time spent in the open arms in the elevated plus-maze test observed

in these mice (**Fig. 5a, b, d, and Supplementary Fig. 5c**). These behavioral improvements were accompanied by a decrease in fibrin accumulation (**Fig. 5e,f**) and a partial restoration of glucose intake into the brain parenchyma (**Fig. 5g**). Aspirin treatment also prevented the hyper-ramification of microglia (**Supplementary Fig. 4a,e**). These results suggest that the prevention of fibrin accumulation in G×E mice afforded by the aspirin treatment is probably important for glucose incorporation into the brain parenchyma, which is necessary for normal brain function.

Vascular injury in postmortem brains of patients with schizophrenia

To confirm whether the fibrin accumulation in the vascular endothelial cells observed in G×E model mice is mirrored in patients with schizophrenia, we examined the fibrin accumulation patterns in human postmortem brains from healthy controls and patients with schizophrenia. Surprisingly, significantly elevated fibrin accumulation was observed in the patients with schizophrenia, both in the white and gray matter, but especially in the white matter (**Fig. 6a–d**). The patients studied here do not necessarily have a tendency toward a high sugar intake, or mutations in the *GLO1* gene, which indicates that the vascular damage detected here in the

brains of patients with schizophrenia is a novel and common phenotype of this psychiatric disorder.

Discussion

In this study, we first generated a schizophrenia-like mouse model by combining *Glo1* heterozygosity with excessive sucrose intake, which means that sucrose over-intake during adolescence is a potential risk factor for the development of schizophrenia. Second, we identified a novel phenotype of schizophrenia, "angiopathy," in our model mice and in patients with schizophrenia. Third, to our surprise, we observed that glucose intake from the plasma into the brain parenchyma was impaired in the model mice. Finally, we found that chronic low-dose aspirin treatment prevented the deposition of fibrin in capillaries, which was accompanied by the improvement of various phenotypes, including cognitive function, and partial amelioration of the abnormal glucose logistics. These results support our hypothesis that excessive sugar consumption leads to the development of schizophrenia and is not merely an abnormal behavior of these patients during the disease process.

Why was a high-sucrose diet toxic for brain functions in *GLO1* heterozygous mice? We

propose the idea that is shown in **Fig. 6e** as diagrams. Sucrose is initially digested to fructose and glucose and that the majority of fructose is converted into glucose in the small intestine and/or is metabolized in the glycolytic pathway in the liver after its incorporation into blood vessels in mice[68,69]. This may explain the observation that the ratio of fructose:glucose in the plasma is about 1:500, both in the fasting and glucose clamping conditions[70]. Despite the low concentration of fructose in the plasma, fructose has a potential to generate AGEs more readily than the same amount of glucose; in addition, it generates pre-AGE carbonyl compounds, such as glyceraldehyde and methylglyoxal[71]. Moreover, in cerebrospinal fluid (CSF), fructose concentration may be controlled by a mechanism that is distinct from that of the plasma, as fructose levels are increased and glucose levels are decreased in this compartment compared with the plasma[70,72]. Fructose-derived pre-AGE carbonyl compounds were detoxified by GLO1 quickly in astrocytes in wild-type mice and probably even in *Glo1* heterozygous mice, because of its strong expression in these cells. However, in the case of endothelial cells and microglia, the metabolism of excessive levels of carbonyl compounds possibly yields an excess of AGEs because of the lack of GLO1 expression, which may induce the pro-inflammatory astrocytic condition via RAGEs or cytokines from microglia[73], leading to nondiabetic angiopathy.

Damaged endothelial cells possibly disturbed normal glucose transportation from the plasma into the brain parenchyma in *Glo1* heterozygous mice that were fed a high-sucrose diet; in contrast, the removal of the angiopathy marker from brain capillaries via aspirin treatment (fibrin accumulation was used here as an angiopathy marker) partially restored the concentration of glucose in the parenchymal intercellular space and prevented many symptoms related with parvalbumin-positive neurons (**Fig. 6e**).

Here, we generated a mouse model of schizophrenia based on the gene × environment interaction approach. The G×E model mice exhibited hyper-locomotion activity and excessive DA release, which were completely recovered by treatment with the dose-dependent partial D2 receptor agonist aripiprazole (**Fig.1h,i**). These abnormalities could be explained by the PV neuron dysfunction that was observed in G×E mice (**Fig. 2**). Genetically induced PV-neuron-specific hypo-function leads to an elevated excitation and inhibition ratio in the ventral hippocampus[74]. Recent studies have suggested that chronic stresses also induce hypo-function of interneurons, including PV neurons, and hyperactivity of excitatory neurons in the hippocampus, cortex, and amygdala[75]. Exacerbated pyramidal neuron activity in the ventral hippocampus may underlie the aberrant modulation of DA release from dopaminergic neurons

of the midbrain after exposure to an adverse environmental stimulus, such as amphetamine[74,76,77]. Moreover, the induction of pan-interneuronal hypo-function (including PV neurons) using the Gad65-Cre-dependent artificial Gαi-coupled receptor (hM4Di) expression triggers hyper-locomotion activity without amphetamine stimulation[30]. In addition, aripiprazole exerts its inhibitory effect toward amphetamine-induced hyperactivity partly through the expression of D2 receptors in PV neurons[74]. In line with these results, the PV neuron dysfunction that was induced by excessive sucrose intake in *Glo1* heterozygous mice may be a major cause of the DA-dependent hyper-locomotion activity observed in these animals (**Figs 1h,i, and 2**). Hyper-dopaminergic activity and PV neuron dysfunction have been reported repeatedly in animal models of, and in patients with, schizophrenia[32,34-37]. Thus, our model mice will be useful to advance our understanding of the pathogenesis and pathophysiology of schizophrenia.

What are the mechanisms that contribute to the induction of the PV neuron dysfunction detected in G×E mice? We observed the inhibition of glucose uptake from the plasma into the brain parenchyma *in vivo* (**Fig. 4g**), which might explain the PV neuron dysfunction observed in our model mice. PV neurons exhibit a low input resistance and high-amplitude rapid after-hyperpolarization[78,79]. This combination of properties generates action potentials at high

frequency, unlike that observed in any other type of neuron. To maintain these properties, PV neurons are predicted to require a high energy expenditure, which is reflected in the enrichment in mitochondria and cytochrome c oxidase observed in these neurons[80]. Therefore, we consider that the effect of the lack of glucose uptake within the brain parenchyma concentrates on PV neuron function. Healthy PV neuron function governs PPI, working memory, amphetamine-induced hyper-locomotion, dopamine (or 3,4-dihydroxyphenylacetic acid (DOPAC)) regulation, and the generation of gamma oscillations[30,32,33,74,81], among other phenotypes; importantly, disruptions of these processes are considered as the core symptoms of schizophrenia. Thus, we propose that impaired glucose intake might have caused the PV neuron dysfunction observed in G×E mice.

In this study, we also identified vascular angiopathy in G×E mice and in the postmortem brains of patients with schizophrenia (**Fig. 6a–d**) and that it may not be restricted to the brain (i.e., it may be a systemic vascular disorder in these patients). In fact, the life expectancy of patients with schizophrenia has been estimated to be 10–25 years shorter than that of the general population[82,83]. Sudden unexpected death, which is mainly caused by vascular problems (including sudden cardiac death), accounts for up to 20% of mortality among patients with

schizophrenia[82,83], which is a high rate even after considering the contribution of both first- and second-generation antipsychotics to sudden cardiac death[82]. Although the angiopathy observed in our model mice was probably caused by the high AGE production ability of the fructose contained in sucrose[84,85], the patients studied here do not necessarily have a record of excessive sucrose intake; i.e., they developed schizophrenia under various stress circumstances, which indicates that a variety of environmental stresses converge to induce angiopathy in these patients. In fact, several studies have reported that many stressors, including social defeat, isolation, and viral infection, are integrated into the vascular burden[86-88]. Interestingly, these stress experiences are also risk factors for schizophrenia, which suggests that angiopathy may be a common trigger of schizophrenic phenotypes.

Chronic treatment with low-dose aspirin exerted a significant and partial effect on the angiopathy (fibrin deposition) and impaired glucose incorporation into the brain parenchyma, with full or partial prevention of the emergence of most of the abnormal behaviors observed in our model mice, including cognitive impairment (**Fig. 5 and Supplementary Fig. 5**). These results can be attributed in part to the three effects of aspirin. The first is a platelet inhibitory action, which is caused by the irreversible inhibition of platelet cyclooxygenase-1 (COX-1)

activity and thromboxane formation, leading to protection against the formation of clots[89,90], which could prevent fibrin deposition in G×E mice (**Fig. 5e,f**). The second is the switch in COX-2 function from a prostaglandin endoperoxide synthase pathway to a lipoxygenase pathway via its acetylation[91,92]. The third is the modulation of oxidative stress. Aspirin-triggered lipoxins reduce the NOX-mediated endothelial production of ROS via the suppression of the redox-sensitive activation of the transcriptional factor NF-κB, which is induced by TNF-α, thrombin, or AGEs[93]. Aspirin also stimulates eNOS production via lysine acetylation, eventually resulting in the induction of heme oxygenase and a decrease in asymmetrical dimethylarginine, which serves as an eNOS inhibitor and improves the anti-oxidative potential of vascular cells[94-97]. Considering the trend of high oxidative stress reported for patients with schizophrenia[9-11], aspirin usage may provide protection against this disease.

Lastly, a high-sucrose diet induced several abnormal phenotypes even in the wild-type mice, such as slightly decreased working memory scores, impaired nest-building, lasting grooming, decrease in the number of PV neurons with elevated gamma oscillation in the home cage condition, etc. (**Fig. 1e–g, 2a–e**). Considering the overall results obtained for the G×E mice, our study may provide important insights for mental health in that an excessive sugar diet

during adolescence may have adverse effects on the human brain function, in addition to the body weight gain and dental caries concerns reported by the WHO.

Figure legends

Figure 1 Generation of novel G×E model mice for schizophrenia and analyses of their behaviors.

(a) Timeline of the experiments. After weaning (P21), mice were fed either a starch diet or a sucrose diet. The behavioral test battery was administered at 2 months of age (at the start of testing) (upper panel). Macronutrient composition of the two diets; the starch diet was used as the control diet, whereas the sucrose diet was used as the experimental diet (middle). We used *Glo1* heterozygous mice to mimic patient with schizophrenia who exhibit decreased GLO1 activity, whereas the high-sucrose intake was used as the environmental risk factor (bottom panel). We investigated four groups of mice: wild-type, starch-fed mice (CTL); wild-type, sucrose-fed mice (Env); *Glo1* heterozygous, starch-fed mice (Gen); and *Glo1* heterozygous, sucrose-fed mice (G×E). **(b–g)** Behavioral analyses of the four groups of mice: wild-type, starch-fed mice (Starch +/+); *Glo1* heterozygous, starch-fed mice (Starch *Glo1*/+); wild-type, sucrose-fed mice (Suc +/+); and *Glo1* heterozygous, sucrose-fed mice (Suc *Glo1*/+) (n = 18–23 mice per group). **(b)** Spontaneous locomotor activity in the open-field test. **(c)** Acoustic startle responses. **(d)** Pre-pulse inhibition for the 70 dB pre-pulse sound levels. **(e)** Object-location test

(to evaluate working memory over 5 min). **(f)** Duration of self-grooming in the home cage. **(g)** Quantification of nest-building skills over 8 h. **(h)** Extracellular concentration of dopamine in the nucleus accumbens, as measured at 20-min intervals using an *in vivo* microdialysis system. Methamphetamine (1.25 mg/kg) was administered i.p. at time 0 (arrow) (n = 8–11 mice per group). **(i–k)** Effects of aripiprazole (Aripi) treatment on abnormal behaviors (n = 16–18 mice per group). **(i)** Quantifications of locomotor activity. **(j)** PPI for the 70 dB pre-pulse sound levels. **(k)** Object-location test. The statistical tests used included the Tukey–Kramer test **(d, e, f, j, and k)** and two-way repeated-measures ANOVA **(b,c,g,h, and i)**; the main effect of group in **b** ($F3, 73 = 6.19$, $P = 0.0008$), **c** ($F3, 63 = 6.75$, $P = 0.0005$), **g** ($F3, 81 = 6.67$, $P = 0.0004$), **h** ($F4, 36 = 14.0374$), and **i** ($F2, 51 = 27.59$, $P < 0.0001$) was followed by Shaffer's multiple comparisons test of genotype groups. **(h)** Bonferroni multiple comparisons test of genotype groups at specific time points, ###$P < 0.001$ for Suc *Glo1*/+ vs. Ctrl (Starch +/+), $$$P < 0.01$ for Starch *Glo1*/+ vs. Ctrl (Starch +/+). Data are means ± s.e.m. *$P < 0.05$, **$P < 0.01$, ***$P < 0.001$; n.s., not significant.

Figure 2 Parvalbumin-positive interneuron dysfunction in G×E mice.

(a) Immunohistochemistry of parvalbumin (PV) in the hippocampal dentate gyrus (DG). **(b)** Number of PV-positive cells in the DG in a (n = 4 slices per group). **(c)** Western blot analysis of the PV protein using tubulin as the internal control. **(d)** Densitometric analysis of the expression levels of the PV protein in c. To evaluate the expression levels of PV, the intensities of the bands in c were divided by their corresponding intensities in the control (tubulin) (n = 3 mice per group). **(e)** Average gamma band power in the home cage and novel object recognition phase (n = 7–8 mice per group). **(f)** Changes in gamma band power from the home cage to the novel object observed in individual mice (n = 7–8 mice per group). The statistical tests used included the Tukey–Kramer test **(b,d, and e)** and two-way repeated-measures ANOVA **(f)**; the main effect of group in **b** ($F3, 73 = 6.19$, $P = 0.0008$), **c** ($F3, 63 = 6.75$, $P = 0.0005$), **g** ($F3, 81 = 6.67$, $P = 0.0004$), **h** ($F4, 36 = 14.0374$), and **i** ($F2, 51 = 27.59$, $P < 0.0001$) was followed by Shaffer's multiple comparison test of genotype groups.

Figure 3 AGE accumulation and pre-inflammatory status of astrocytes in G×E mice.

(a) Images of the results of immunohistochemistry for AGEs in the medial prefrontal cortices. **(b)** Measurement of the area covered by AGEs in a, where the area is above the appropriate

threshold of pixel intensity in each image (n = 3 slices per group). The mean intensity of the entire image was measured in each section. **(c–e)** Immunohistochemical data including images of colocalization between tomato-lectin (endothelial cell marker) or Aldh1l1 (astrocyte marker) and AGEs. **(f,g)** Plots of pixel intensities along the white arrow in d for f, and e for g. The black arrows in f indicate colocalization points of lectin and AGEs. **(h)** Immunohistological images of GFP-positive astrocytes in the hippocampal CA1 region. **(i)** Number of GFP-positive cells in each image presented in h. No significant differences were observed among the groups. **(k)** Mean fluorescent intensities of 10 randomly selected cells per image from the hippocampal CA1 region of four independent mice. The statistical tests used included the Tukey–Kramer test in **b**,**i**, and **j**. $^{**}P < 0.01$; $^{***}P < 0.001$.

Figure 4 Angiopathy and impaired glucose incorporation observed in G×E mice.

(a,b) Venn graph showing the overlap in the genes that exhibited >2-fold **(a)** or <0.5-fold **(b)** expression levels compared with the CTL group using PFC samples (n = 3 per group). **(c)** Immunohistochemical images of fibrin and the endothelial cell marker tomato-lectin. **(d)** Measurement of the area covered with fibrin in c, where the area is above the appropriate

threshold of pixel intensity in each image (n = 3 slices per group). The mean intensity of the entire image was measured for each section. **(e)** Co-immunohistochemical images of tomato-lectin with fibrin in the medial prefrontal cortices. **(f)** Plots of pixel intensities along the yellow arrow in e. **(g)** Extracellular concentrations of glucose in the dialysis buffer at each time point (1 h collection after 16 h of fasting; for 1 h after eating a 0.05 g diet; for 1 h from 1 h after eating a 0.05 g diet) (n = 5–6 mice per group). **(h)** Plasma glucose levels in wild-type and *Glo1* heterozygous mice (n = 6–7 mice per group). The first measurement was performed after 16 h of fasting, and the second blood collection was performed 30 min after eating a 0.05 g diet. No significant differences were observed among the groups. **(i)** Fasting plasma insulin levels in wild-type and *Glo1* heterozygous mice. No significant differences were observed between the groups (n = 5–6 mice per group). Further, the 0.05 g diet we used in g, h, and i were daily eaten by mice in each group (0.05 g sucrose for the daily sucrose eating group and 0.05 g starch for the daily starch eating group). The statistical tests used included two-way repeated-measures ANOVA in **g** and **h**; main effect of group in **g** ($F3, 23 = 5.7851$, $P = 0.0042$) and **h** ($F3, 23 = 2.9734$, $P = 0.0528$), and the Tukey–Kramer test in **d** and **i**. The data are presented as the mean ± s.e.m. $^{**}P < 0.01$; $^{*}P < 0.05$.

Figure 5 Protective effects of low-dose aspirin against the impairments observed in G×E mice. **(a–d)** Results of behavioral tests that were performed to evaluate the effects of aspirin treatment (n = 12–21 mice per group). **(a)** Quantifications of spontaneous locomotor activity using the open-field test. **(b)** Pre-pulse inhibition test at 70 dB. **(c)** Object-location test (to evaluate working memory over 5 min). **(d)** Quantification of nest-building skills over 8 h (n = 12–21 mice per group). **(e)** Immunohistochemical images of fibrin and the endothelial cell marker tomato-lectin. **(f)** Measurement of the area covered with fibrin in **e**, in which the area is above the appropriate threshold of pixel intensity in each image (n = 3 slices per group). The mean intensity of the entire image was measured for each section. **(g)** Extracellular concentrations of glucose in the dialysis buffer at each time point (1 h collection after 16 h of fasting, for 1 h after eating a 0.05 g diet, for 1 h from 1 h after eating a 0.05g diet) (n = 4–6 mice per group). The statistical tests used included the Tukey–Kramer test in **b**, **c**, and **f**; two-way repeated-measures ANOVA in **a** and **d**; main effect of group in **a** ($F2, 50 = 6.4385$, $P = 0.0033$), **d** ($F2, 49 = 8.0315$, $P = 0.001$) and **g** ($F2, 17 = 6.1758$, $P = 0.0096$). The data are presented as the mean ± s.e.m. *$P < 0.05$; **$P < 0.01$; ***$P < 0.01$.

Figure 6 Vascular injury in postmortem brains from individuals with schizophrenia.

(a, c) Representative immunohistochemical images of fibrin (gray) and the endothelial cell marker tomato-lectin (green) in postmortem brains from healthy controls and patients with schizophrenia: white matter **(a)** and gray matter **(c)**. **(b, d)** Measurement of the area covered with fibrin in **a** and **c**, in which the area is above the appropriate threshold of pixel intensity in each image (n = 10 slices per group). The mean intensity of the entire image was measured for each section. The statistical tests used included the Tukey–Kramer test in **b** and **d**. The data are presented as the mean ± s.e.m. $*P < 0.05$; $***P < 0.01$. **(e)** Diagrams describing the hypothesis that was proposed to explain the phenomena observed in CTL mice (left) and in G×E mice (right). (see the Discussion section for details).

Supplementary Figure Legends

Supplementary Figure 1 Characterization of Glo1 expression level and mice in the four groups.

(a) Western blot analysis of the GLO1 protein using tubulin as an internal control. The cerebral cortex, including the hippocampus, was used as the loading sample. **(b)** Densitometric analysis of the expression levels of the GLO1 protein (Starch +/+, n = 3; Starch *Glo1*/+, n = 4; Suc +/+, n = 3; Suc *Glo*1/+, n = 4). To evaluate the expression levels of GLO1, the intensities of bands shown in a were divided by their corresponding intensities in the control (tubulin). **(c)** Body weight trajectories. No significant differences were observed among the groups (n = 9–10 mice per group). The statistical tests used included Dunnett's test in **b** and two-way repeated-measures ANOVA in c; main effect of group ($F_{3, 33} = 1.7512$, $P = 0.1757$). The data are presented as the mean ± s.e.m. *$P < 0.05$.

Supplementary Figure 2 Behavioral phenotypes and the effect of aripiprazole treatment.

(a) Elevated plus-maze test (to evaluate anxiety). **(b)** Interaction time with an empty cylinder (object) or a mouse placed in the cylinder in the social interaction test. No differences were detected in the social interaction test among the four groups. **(c–f)** Effects of aripiprazole treatment on the acoustic startle response **(c)**, self-grooming **(d)**, elevated plus-maze test **(e)**, and nest-building skills **(f)**. The abnormal behaviors of G×E mice in these tests were not improved

by aripiprazole treatment. The statistical tests used included the Tukey–Kramer test in **a**,**b**,**d**, and **e**; and two-way repeated-measures ANOVA in **c** and **f**; main effect of group in **c** ($F2, 35 = 8.557$, $P = 0.0009$) and **f** ($F2, 47 = 14.6637$, $P = 0.004$). The data are presented as the mean ± s.e.m. $*P < 0.05$; $**P < 0.01$; $***P < 0.001$.

Supplementary Figure 3 Investigation of GLO1 localization in the cerebral cortices in sucrose-fed wild-type mice.

(a–f) Localization of GLO1 in astrocytes. **(a)** Immunohistological images of GLO1 coimmunostaining with an astrocyte marker (ALDH1L1) or with an endothelial cell marker (tomato-lectin). **(b)** Merged image of GLO1 and ALDH1L1 in a. The yellow arrows in b indicate cells with colocalization of GLO1 and ALDH1L1. **(c)** Merged image of GLO1 and lectin in a. The white arrows point to the representative GLO1-positive cells located close to the endothelial cells. **(d,e)** Higher-magnification images of GLO1 coimmunostaining with ALDH1L1 or with tomato-lectin from a different focal plane. **(e)** Merged image of GLO1 and ALDH1L1 in d. **(f)** Plots of pixel intensities along the yellow arrow in e. The black arrows indicate the areas of colocalization of GLO1 and ALDH1L1. **(h)** Merged image of GLO1 and

tomato-lectin in **g**. **(i)** Plots of pixel intensities along the white arrow in h. Unlike that observed in f, the GLO1 expression pattern showed a similar tendency to that of tomato-lectin expression, while ALDH1L1 exhibited a different expression pattern. **(j)** Coimmunostaining of GLO1 with the neuronal marker NeuN and the microglial marker IBA1. **(k)** Merged image of GLO1 and NeuN in j. The yellow arrows indicate neurons with mild GLO1 immunoreactivity. **(l)** Merged image of GLO1 and IBA1 in j. The white arrows indicate microglia with weak GLO1 immunoreactivity. **(m)** GLO1 immunostaining together with DAPI staining in *Glo1* homozygous mice.

Supplementary Figure 4 Fructose-derived AGE accumulation in microglia in sucrose-fed mice.

(a,b) Immunohistochemical images of the microglial marker (IBA1) and AGE4 in the CA1 region. **(c)** Merged image of AGE4 and IBA1. **(d)** Higher-magnification images of AGE4 coimmunostaining with IBA1. **(e)** Number of protrusions in each IBA1-positive cell in each image in a. Mean number of protrusions in five randomly selected cells per image from three independent mice. **(f)** Measurement of the area covered with AGEs in a, in which the area is

above the appropriate threshold of pixel intensity in each image. The mean intensity of the entire image was measured for each section (n = 4–5 slices per group). The statistical tests used included the Tukey–Kramer test in **e** and **f**. **P* < 0.05; ***P* < 0.01; ****P* < 0.001.

Supplementary Figure 5 Protective effects of aspirin against the development of abnormal behaviors in G×E mice.

(a–c) Effects of aspirin treatment on the acoustic startle response **(a)**, self-grooming **(b)**, and elevated plus-maze **(c)** tests. The administration of aspirin led to effective prevention of deficits in grooming duration and partially ameliorated the decline in acoustic responses; it also improved the time spent in the open arms in the elevated plus-maze test in G×E mice. The statistical tests used included two-way repeated-measures ANOVA in **a** ($F2, 42 = 8.0903$, $P = 0.0011$) and the Tukey–Kramer test in **b** and **c**. The data are presented as the mean ± s.e.m. **P* < 0.05; ****P* < 0.001.

Methods

Animals

All experimental procedures were approved by the Animal Experimentation Ethics Committee of the Tokyo Metropolitan Institute of Medical Science (49040). All mice were maintained with a 12:12 h light/dark cycle (lights on at 8:00 AM). All efforts were made to minimize the number of animals used and their suffering. The generation of *Glo1* knock out mice will be described by K.T. in detail elsewhere. In brief, *Glo1*-trapped ES cell lines from the International Gene Trap Consortium were used for the generation of thee mice, which were backcrossed to C57BL/6 mice. GFAP-GFP mice were used to monitor the activation of astrocytes[50,51]. Male mice were used exclusively in the behavioral tests and their weights were measured. Mice of both sexes were used in histological, biochemical, and physiological experiments.

Diet preparation

The two diets used in this study were newly created in collaboration with Oriental Yeast Co., Ltd. (Tokyo, Japan). We named the sucrose diet as HSD-70 (# OYC 2405100) and the starch diet as HCD-70 (# OYC 2405000). They were composed of the same caloric percentages of

carbohydrates, fat, and proteins. The control diet used starch as a source of carbohydrates, whereas the experimental diet used sucrose as the carbohydrate source. We created the sucrose diet with isomerized sugars in mind.

Drug preparation

Aripiprazole was dissolved in acetic acid and diluted with water to 3.5 mg/L (0.5 mg/kg/day). The final acetic acid concentration in the drinking water was 0.7%. Aspirin was dissolved in ethanol and diluted with water to 70 mg/L (1 mg/kg/day). The final ethanol concentration in the drinking water was 0.15%. As a result of our quantification, we assumed that the mice drank an average of 5 ml of water per day.

Behavioral tests

Mice were habituated in the behavioral room for over 30 min before each test began. The behavioral tests were performed in the following sequence of increasing stress intensity: elevated plus-maze test; grooming test; nest-building test; open-field test; object-location test; social interaction test; and PPI test. The apparatuses were cleaned with 70% ethanol and water,

and the subsequent test session started after the ethanol vapor odors had disappeared and the apparatuses had dried.

For the elevated plus-maze (EPM) test, the apparatus consisted of two open arms and two closed arms (EPM-04M, Muromachi, Japan): two opposing open arms (297 × 54 mm) and two closed arms (300 × 60 × 150 mm) that extended from a central platform (60 × 60 mm) that was elevated 400 mm above the floor. Each mouse was placed on the central platform facing a closed arm and was allowed to explore the maze freely for 10 min. Entry into an arm was defined as the entry of all four paws into the arm. The time spent in the open arms over 10 min was recorded.

For the self-grooming test, all mice housed in the same home cage were moved once into a new cage for 10 min. Each mouse was then placed individually in a standard mouse home cage (31 × 16.5 ×14 cm) illuminated at around 200 lux. After a 10 min habituation period, each mouse was scored using a stopwatch for 10 min regarding the cumulative time spent grooming all body regions[98]. The self-grooming behavior is conserved across species. In humans, the self-grooming behavior stems from pathological factors; for example, it occurs during stressful conditions or in certain neuropsychiatric disorders, including schizophrenia[98].

For the nest-building test, 200 g of corncob was spread across the bottom of each cage, for bedding, and a square-shaped piece of cotton was placed in the center of the cage. The subject was individually located in the cage above. Photos of the nest that was created using the cotton were acquired every 2 h over 8 h, and the nest-building process was evaluated by measuring the proportion of loose cotton: 1 point for 25% weight (Wt%) loosened; 2 points for 50 Wt% loosened; 3 points for 75 Wt% loosened; and 4 points for 100 Wt% loosened. After 8 h, we checked the shape of the nest and added 1 point if the mice had finished nest construction, meaning that the nest had a bird's nest-like shape. The temperature of the room was maintained at 25°C during nest-building. We performed this test under illumination of 150–180 lux. The nest-building behavior is an indicator of well-being in mice[99] and is also used as an indicator of negative symptoms in these animals[100,101].

For the open-field (OF) test, each mouse was placed in the center of the apparatus (40 × 40 × 40 cm; 150–180 lux illumination) and was allowed to move freely for 10 min. The behavior of each mouse was monitored using a CCD camera mounted on the ceiling of the rack of the OF. The total distance traveled (cm) was measured.

For the object-location test, which was used to evaluate working memory[102], mice first

explored the box that was used for the OF test, and two identical objects (objects A and B) were placed in two corners of the box. The objects were placed 5 cm from each wall. We used 500 mL PET bottles filled with blue-colored water as objects. After a 10 min learning period, the mice were returned to their home cage for 5 min and were then placed back in the box, in which Object A had been moved to a new corner (Object A'); the animals were allowed to explore the box for 5 min. The score on this test was calculated as a discrimination index that represented working memory and was calculated using the following equation: Discrimination Index = (Novel Object A'–Familiar object B) / (Novel Object A' + Familiar object B). The OTC was performed under illumination of 10–15 lux.

For the social interaction test, sociability was assessed as described earlier[87] using a Sociability Apparatus (SC-03M, Muromachi). The time spent sniffing mice and objects was manually scored by referring to the video that was recorded using an overhead color USB camera (aa000080a02, Iroiro House). Stimulus mice were habituated to the apparatus and to the enclosure cup for 30 min per day for 2 days. 129Sv/SvJcl mice were used as stimulus animals and were matched to the subject mice by sex and age. The location (left or right) of the novel object and novel mouse alternated across subjects. The subject mouse was allowed to acclimate

to the apparatus for 20 min before the sociability test: 10 min in the central chamber with the doors closed, followed by 10 min in the empty arena with the doors open. The subject was then briefly confined to the center chamber while a novel stimulus mouse was enclosed in the empty enclosure cup that was placed on one of the side chambers, with another empty enclosure cup being placed on the other side of the chamber. Then, the subject was allowed to approach freely for 10 min the novel object or mouse that was placed in each chamber. The location (left or right) of the novel object and novel mouse alternated across subjects.

For the acoustic startle response and pre-pulse inhibition (PPI) tests, an SR-LAB-Startle Response System (San Diego Instruments) was used to detect acoustic startle reflexes. Startle responses were measured using five stimuli intensities (10 times each of 80, 90, 100, 110, and 120 dB for 40 ms) under the condition of white noise stimulus (65 dB). The stimuli were presented in quasi-random order at random inter-trial intervals (10–20 s). In the PPI session, mice experienced two trial types: 1) no stimulus, startle stimulus (120 dB, 40 ms) only, 2) pre-pulse stimulus, 70 dB (20 ms; lead time, 100 ms), and startle stimulus, 120 dB. Each trial was repeated 10 times in quasi-random order at random inter-trial intervals (10–20 s). PPI was defined as the percent decline in the startle response and was calculated using the following

equation: 100–[(120 dB startle amplitude after any pre-pulse) / (120 dB startle amplitude only)] × 100.

Immunohistochemistry

After transcardial perfusion with PBS and 4% paraformaldehyde (PFA), mouse whole-brains were collected and post-fixed at 4°C overnight. The brains were then cryoprotected in 20% sucrose at 4°C overnight. Serial coronal sections (50 μm) were cut using a cryostat (CM3050 S; Leica Microsystems). The antigens in the tissues were reactivated by heating in HistoVT One solution (Nakalai Tesque) for 30 min at 70°C using a water bath. Sections were permeabilized with 0.2% Triton X-100 and 1% Block Ace (DS Pharma Biomedical) in PBS for 30 min at room temperature and incubated overnight with primary antibodies at room temperature. For immunohistochemistry in postmortem paraffin-embedded human brain tissues, paraffin blocks including BA9 regions were sliced into 10 μm sections, deparaffinized with xylene, and rehydrated with decreasing concentrations of ethanol in water. The antigens in the tissues were reactivated by heating in HistoVT One solution for 30 min at 90°C using a water bath. Sections were treated with TrueBlack to quench lipofuscin (TrueBlackTM Lipofuscin Autofluorescence

Quencher, Biotium Inc.) for 30 s at room temperature, followed by blocking with 1% Block Ace (DS Pharma Biomedical) in PBS for 30 min at room temperature. Thereafter, mouse and human brain sections were subjected to the same procedures. The following primary antibodies were diluted in PBS including 0.4% Block Ace: goat anti-parvalbumin (Frontier institute, PV-Go-Af860; 1:2000), mouse anti-ALDH1L1 (Abnova, H00010840-M01; 1:200), FITC-conjugated tomato-lectin (VECTOR, FL-1171; 1:200), chick anti-GFP (Abcam, ab13970; 1:500), goat anti-IBA1 (Abcam, ab48004; 1:100), mouse anti-NeuN (Millipore, MAB377; 1:500), rabbit anti-AGE (Abcam, ab23722; 1:2000), rabbit anti-IBA1 (Wako, WDJ3047; 1:300), and rabbit anti-fibrin (Dako, A0080, 1:500). Sections were then washed three times with PBS-0.05% Tween-20, incubated for 2 h with fluorochrome-conjugated secondary antibodies in PBS including 0.4% Block Ace, and washed an additional three times. For enhanced immunostaining, treatment with 3% H_2O_2 in PBS for 20 min was administered after the reactivation step. Sections were washed once before and once after the H_2O_2 treatment using PBS. Anti-IgG antibodies conjugated to biotin (Vector, 1:200) were used as secondary antibodies to rabbit anti-GLO1 (Novusbio, NBP2-75514, 1:1500), and rabbit anti-AGE4 (Trans Genic Inc, 14B5, 1:400) antibodies, followed by washing using the procedure described for the

normal secondary antibodies. Sections were incubated with streptavidin-conjugated HRP (Jackson ImmunoResearch, 1:200) for 120 min and, after washing three times with PBS-0.05% Tween-20, the TSA Plus Fluorescence System (PerkinElmer) was used to detect HRP activity. Finally, all types of sections were treated with DAPI (Nacalai Tesque), for nuclear staining, washed three additional times, mounted in Permaflow (Thermo Scientific), and observed using a FluoView® FV3000 Confocal Laser Scanning Microscope (Olympus). Counting of GFP-, AGE-, AGE4-, or fibrin-positive cells or measurement of areas that were positive for these proteins were performed in a fixed area using ImageJ version 2.0.0-rc-59/1.51n.

Immunoblotting

Extracts from mouse hippocampi were homogenized in lysis buffer containing 40 mM Tris (Tris Base), 0.4% SDS, 0.01 M EDTA (pH 8.0), 8 M urea, and 1 mM PMSF. The protein content in total cell lysates was quantified using a DC Protein Assay Kit (Bio-Rad) and 30 μg of total protein per lane was run in SDS–PAGE and transferred to PVDF membranes (Millipore). Membranes were blocked with TBST buffer (1.37 M NaCl, 2.7 mM KCl, and 0.25 M Tris, pH 8.0) including 0.2% Triton X-100 and 5% BSA for 30 min at room temperature with slow

shaking, followed by incubation overnight with primary antibodies in TBST including 2% BSA at 4°C. The primary antibodies used were rabbit anti-GLO1 (Santa Cruz, sc-67351; 1:1000), mouse-anti-parvalbumin (Swant, PV-235; 1:1000), and mouse-anti-tubulin (Santa Cruz, sc-32293; 1:10000). After washing three times with TBST, membranes were incubated with the secondary antibody (HRP conjugated anti-mouse or rabbit IgG antibody, GE Healthcare; 1:2000) in TBST including 2% BSA. After washing three times with TBST, blots were processed for chemiluminescence using standard protocols (ECL Prime Western Blotting Detection Regent #RPN2236, GE Healthcare) and signal detection was achieved using an LAS 4000 Imager (Fuji Film).

Microdialysis

We used an in vivo microdialysis system for the measurement of dopamine concentration and the collection of brain parenchyma lysates, as described by Tellez[103]. After anesthesia with an intraperitoneal injection of ketamine (80 mg/kg)/xylazine (16 mg/kg), mice were fixed in a stereotaxic apparatus (Narishige) and a microdialysis guide cannula (CXG-8, Eicom) was implanted in the medial prefrontal cortex (mPFC) (antero-posterior (AP), +1.8 mm;

medio-lateral (ML), ±0.15 mm; dorso-ventral (DV), −1.5 mm from bregma) or nucleus accumbens (NAc) (AP, +1.5 mm; ML, ±0.6 mm; DV, −3.5 mm from bregma). After recovery for at least 10 days, a microdialysis probe (CX-I-8-01 for the mPFC and CX-I-8-02 for NAc; Eicom) was inserted through the guide cannula. After insertion, probes were connected to a syringe pump and perfusion was performed at 2 μl/min for NAc and 0.5μl/min for mPFC using Ringer's solution (147 mM NaCl, 4 mM KCl, and 2.3 mM $CaCl_2$). Dialysate samples were collected every 10 min and automatically loaded onto an HTEC-500EPS HPLC unit (Eicom). Constant 5-HT concentration in three consecutive collection periods was confirmed, to rule out blood contamination, before starting the measurements of dopamine concentration or the collection of dialysates. Analytes were then separated on an affinity column (PP-ODS III, Eicom) and compounds were subjected to redox reactions within an electrochemical detection unit (amperometric DC mode; applied potential range, 450 mV). The resulting chromatograms were analyzed using an EPC-500 data processor (Eicom) and actual sample concentrations were computed based on the peak heights obtained from a standard curve that was prepared from 0.01, 0.1, and 1 pg dopamine in standard solutions (Sigma). The locations of the microdialysis probes were confirmed histologically.

Electroencephalography (EEG) recordings

For behavioral and video/EEG monitoring, after anesthesia via intraperitoneal injection of ketamine (80 mg/kg)/xylazine (16 mg/kg), mice were fixed in a stereotaxic apparatus (Narishige, Japan) and EEG and electromyography (EMG) electrodes were implanted. The EEG electrodes were gold-coated stainless Steel screws (SUS303) soldered with lead wires (ANE-0190, Adler's Nest, Japan) that were implanted epidurally over the left frontal cortex (AP, 1 mm; ML, 1 mm) and the bilateral parietal cortex (AP,–2 mm; ML, ±2 mm). All wires were soldered to a multichannel electrical connector (R833-83-006-001, TOKIWA SHOKO, Japan). The left parietal cortex electrode was used as a reference electrode. The signal difference between the frontal cortex and the right parietal cortex was used as EEG data. The EMG electrodes were lead wires that were placed bilaterally into the trapezius muscle. After recovery for at least 10 days, EEG/EMG signals were amplified and filtered (EEG: 1.5–1000 Hz; EGM: 15–3000 Hz) using an amplifier (MEG-6116, NIHON KOHDEN), digitized at a sampling rate of 200 Hz, recorded with a data acquisition system (PowerLab 8/30, ADInstruments), and analyzed using the LabChart Software (ADInstruments). Behavioral activities were recorded using a USB

camera (aa000080a02, Iroiro House, Japan). The behavioral and electrophysiological activities of the mice were recorded in an OF chamber (20 × 20 × 26 cm). Home cage activities were recorded after a 2 h habituation period. Subsequently, an object (an empty 100 ml DURAN bin) was placed in one of the corners of the OF chamber to induce exploring activities for a novel object, which were recorded. The selection of home cage EEG data for 2 min was made from the awaking period and was confirmed by the presence of clear EMG signals and movement images from an offline video camera analysis ("home cage activity"). The 30 s that preceded the first contact with the novel object were analyzed for object recognition ("object activity"). Recordings were converted into power spectra by a fast Fourier transform (FFT) algorithm with a Hann cosine-bell window and a 50% overlap between windows of 5 s periods. FFT was conducted with a 1024 point FFT, to obtain a resolution of 0.512 Hz. The total signal amplitude or the power in V2 in each 5 s period was taken to represent the magnitude of the power of each frequency. The grouped power spectra were averaged at frequency ranges that were divided into four groups, as follows: 1–4 Hz (delta range), 5–10 Hz (theta range), 30–45 Hz (low gamma range), and 55–80 Hz (high gamma range). The power values detected at each frequency range for 30 s were further averaged over 30 s of total EEG power using the average values, to remove

potential noise. The analysis was performed using a custom software written by MATLAB (R2019b; MathWorks).

Transcriptome analysis

mRNA samples were obtained from the prefrontal cortices of mice in the four groups: wild-type, starch-fed mice (CTL); wild-type, sucrose-fed mice (Env); *Glo1* heterozygous, starch-fed mice (Gen); and *Glo1* heterozygous, sucrose-fed mice (G×E). Three independent total RNA samples from each group were mixed and purified using an RNeasy Mini Kit (Qiagen). RNA quality was assessed using a 2100 bioanalyzer (Agilent Technologies). Cy3-labeled cRNA was prepared using a Low Input Quick Amp Labeling Kit in accordance with the manufacturer's protocol (Agilent Technologies). Samples were hybridized to the SurePrint G3 Mouse Gene Expression v2 Microarray (G4852B; Agilent Technologies), washed, and then scanned using a SureScan Microarray Scanner (Agilent Technologies). The microarray images were analyzed using the Feature Extraction software using default setting for all parameters (Agilent Technologies). Data from each microarray analysis were normalized by shift to the 75th percentile without baseline

transformation. The microarray data were deposited in GEO under the GSE141829 accession number.

Insulin and glucose measurements

Blood plasma was collected from the mouse cheek as described by Golde[104]. Plasma glucose concentration was measured using a Precision-Neo blood glucose meter (#71386-80, Abbott Japan). Plasma insulin concentration was measured using an ELISA kit (#M1102, MORINAGA), and glucose concentration in the dialysate samples was measured using another ELISA kit (#ab65333, Abcam), according to manufacturers' guidelines. Data were collected on a microplate reader (Varioskan, Thermo Fisher Scientific).

Human postmortem brain tissue collection

Postmortem brain tissues from patients with schizophrenia were obtained from the Fukushima Brain Bank at the Department of Neuropsychiatry, Fukushima Medical University. Postmortem brain tissues from control subjects were obtained from the Section of Pathology, Fukushima Medical University Hospital. The use of postmortem human brain tissues in the present study

was approved by the Ethics Committee of Fukushima Medical University (No.1685) and Tokyo Metropolitan Institute of Medical Science (No. 18-20) and complied with the Declaration of Helsinki and its later amendments. All procedures were carried out with the informed written consent of the next of kin. The detailed demographic information of the 10 subjects with schizophrenia and 10 age- and sex-matched control subjects from whom brain tissues were collected in this study is provided in **Supplementary Table 3**. There were no between-group differences in sex (Fisher's exact test, $P = 0.65$), age (Welch's *t*-test, $P = 0.34$), and postmortem interval (PMI) (Welch's *t*-test, $P = 0.89$). Each patient with schizophrenia fulfilled the diagnostic criteria established by the American Psychiatric Association (Diagnostic and Statistical Manual of Mental Disorders, DSM-IV) and did not have a past history of other neurological disorders or substance abuse. In addition, none of the control subjects had any record of mental disorders, neurological disorders, or substance abuse. All brain tissue blocks were fixed in 10% formalin, embedded in paraffin, and sliced into 10 μm sections. Tissue blocks were obtained from the dorsolateral prefrontal cortex (BA9).

Statistical analyses

Data were analyzed using the Tukey–Kramer test or two-way repeated-measures ANOVA with Shaffer's procedure for multiple comparisons test, respectively. GLO1 immunoblotting data were analyzed using Dunnett's test. Postmortem brain data were analyzed using Welch's *t*-test. Regarding the behavioral results of Starch +/+ and Suc *Glo*1/+, the data of the same group were reused according to the 3R rule. The number of groups used can be found in the legend to each figure. Significance was set at $P < 0.05$ (n.s., not significant).

1. WHO-Guideline. Sugar Intake for adults and children. (2015).
2. Lazar, M.A. How obesity causes diabetes: not a tall tale. *Science* **307**, 373-375 (2005).
3. Hall, M.E.*, et al.* Obesity, hypertension, and chronic kidney disease. *Int J Nephrol Renovasc Dis* **7**, 75-88 (2014).
4. Johnson, R.J.*, et al.* Potential role of sugar (fructose) in the epidemic of hypertension, obesity and the metabolic syndrome, diabetes, kidney disease, and cardiovascular disease. *Am J Clin Nutr* **86**, 899-906 (2007).
5. Segal, M.S., Gollub, E. & Johnson, R.J. Is the fructose index more relevant with regards to cardiovascular disease than the glycemic index? *Eur J Nutr* **46**, 406-417 (2007).
6. Brandon, N.J. & Sawa, A. Linking neurodevelopmental and synaptic theories of mental illness through DISC1. *Nat Rev Neurosci* **12**, 707-722 (2011).
7. Kirkbride, J.B.*, et al.* Heterogeneity in incidence rates of schizophrenia and other psychotic syndromes: findings from the 3-center AeSOP study. *Arch Gen Psychiatry* **63**, 250-258 (2006).

8. Kirkbride, J.B., *et al.* Neighbourhood variation in the incidence of psychotic disorders in Southeast London. *Soc Psychiatry Psychiatr Epidemiol* **42**, 438-445 (2007).
9. Ciobica, A., Padurariu, M., Dobrin, I., Stefanescu, C. & Dobrin, R. Oxidative stress in schizophrenia - focusing on the main markers. *Psychiatr Danub* **23**, 237-245 (2011).
10. Kim, E., *et al.* Validation of oxidative stress assay for schizophrenia. *Schizophr Res* **212**, 126-133 (2019).
11. Bitanihirwe, B.K. & Woo, T.U. Oxidative stress in schizophrenia: an integrated approach. *Neurosci Biobehav Rev* **35**, 878-893 (2011).
12. Wautier, J.L., *et al.* Advanced glycation end products (AGEs) on the surface of diabetic erythrocytes bind to the vessel wall via a specific receptor inducing oxidant stress in the vasculature: a link between surface-associated AGEs and diabetic complications. *Proc Natl Acad Sci U S A* **91**, 7742-7746 (1994).
13. Miyata, T. Alterations of non-enzymatic biochemistry in uremia, diabetes, and atherosclerosis ("carbonyl stress"). *Bull Mem Acad R Med Belg* **157**, 189-196; discussion 196-188 (2002).
14. Arai, M., *et al.* Enhanced carbonyl stress in a subpopulation of schizophrenia. *Arch Gen Psychiatry* **67**, 589-597 (2010).
15. Miyashita, M., *et al.* Clinical features of schizophrenia with enhanced carbonyl stress. *Schizophr Bull* **40**, 1040-1046 (2014).
16. Thornalley, P.J., *et al.* Quantitative screening of advanced glycation endproducts in cellular and extracellular proteins by tandem mass spectrometry. *Biochem J* **375**, 581-592 (2003).
17. Toyosima, M., *et al.* Schizophrenia with the 22q11.2 deletion and additional genetic defects: case history. *Br J Psychiatry* **199**, 245-246 (2011).
18. Ratliff, J.C., *et al.* The effect of dietary and physical activity pattern on metabolic profile in individuals with schizophrenia: a cross-sectional study. *Compr Psychiatry* **53**, 1028-1033 (2012).
19. Peet, M. International variations in the outcome of schizophrenia and

the prevalence of depression in relation to national dietary practices: an ecological analysis. *Br J Psychiatry* **184**, 404-408 (2004).

20. Kahn, R.S. & Keefe, R.S. Schizophrenia is a cognitive illness: time for a change in focus. *JAMA Psychiatry* **70**, 1107-1112 (2013).
21. Kahn, R.S.*, et al.* Schizophrenia. *Nat Rev Dis Primers* **1**, 15067 (2015).
22. Howes, O.D.*, et al.* Molecular imaging studies of the striatal dopaminergic system in psychosis and predictions for the prodromal phase of psychosis. *Br J Psychiatry Suppl* **51**, s13-18 (2007).
23. Laruelle, M.*, et al.* Single photon emission computerized tomography imaging of amphetamine-induced dopamine release in drug-free schizophrenic subjects. *Proc Natl Acad Sci U S A* **93**, 9235-9240 (1996).
24. Oades, R.D., Taghzouti, K., Rivet, J.M., Simon, H. & Le Moal, M. Locomotor activity in relation to dopamine and noradrenaline in the nucleus accumbens, septal and frontal areas: a 6-hydroxydopamine study. *Neuropsychobiology* **16**, 37-42 (1986).
25. Kelly, P.H., Seviour, P.W. & Iversen, S.D. Amphetamine and apomorphine responses in the rat following 6-OHDA lesions of the nucleus accumbens septi and corpus striatum. *Brain Res* **94**, 507-522 (1975).
26. Koob, G.F., Stinus, L. & Le Moal, M. Hyperactivity and hypoactivity produced by lesions to the mesolimbic dopamine system. *Behav Brain Res* **3**, 341-359 (1981).
27. de Bartolomeis, A., Tomasetti, C. & Iasevoli, F. Update on the Mechanism of Action of Aripiprazole: Translational Insights into Antipsychotic Strategies Beyond Dopamine Receptor Antagonism. *CNS Drugs* **29**, 773-799 (2015).
28. Keefe, R.S.*, et al.* Neurocognitive effects of antipsychotic medications in patients with chronic schizophrenia in the CATIE Trial. *Arch Gen Psychiatry* **64**, 633-647 (2007).
29. Keshavan, M.S., Lawler, A.N., Nasrallah, H.A. & Tandon, R. New drug developments in psychosis: Challenges, opportunities and strategies. *Prog Neurobiol* **152**, 3-20 (2017).

30. Nguyen, R. Investigating the Roles of Parvalbumin and Cholecystokinin Interneurons of the Ventral Hippocampus and Medial Prefrontal Cortex in Schizophrenia-Related Behaviours. (2018).
31. Murray, A.J., *et al.* Parvalbumin-positive interneurons of the prefrontal cortex support working memory and cognitive flexibility. *Sci Rep* **5**, 16778 (2015).
32. Fujihara, K., *et al.* Glutamate Decarboxylase 67 Deficiency in a Subset of GABAergic Neurons Induces Schizophrenia-Related Phenotypes. *Neuropsychopharmacology* **40**, 2475-2486 (2015).
33. Korotkova, T., Fuchs, E.C., Ponomarenko, A., von Engelhardt, J. & Monyer, H. NMDA receptor ablation on parvalbumin-positive interneurons impairs hippocampal synchrony, spatial representations, and working memory. *Neuron* **68**, 557-569 (2010).
34. Beasley, C.L. & Reynolds, G.P. Parvalbumin-immunoreactive neurons are reduced in the prefrontal cortex of schizophrenics. *Schizophr Res* **24**, 349-355 (1997).
35. Hashimoto, T., *et al.* Gene expression deficits in a subclass of GABA neurons in the prefrontal cortex of subjects with schizophrenia. *J Neurosci* **23**, 6315-6326 (2003).
36. Thompson, M., Weickert, C.S., Wyatt, E. & Webster, M.J. Decreased glutamic acid decarboxylase(67) mRNA expression in multiple brain areas of patients with schizophrenia and mood disorders. *J Psychiatr Res* **43**, 970-977 (2009).
37. Nguyen, R., *et al.* Parvalbumin and GAD65 interneuron inhibition in the ventral hippocampus induces distinct behavioral deficits relevant to schizophrenia. *J Neurosci* **34**, 14948-14960 (2014).
38. Buzsaki, G. & Wang, X.J. Mechanisms of gamma oscillations. *Annu Rev Neurosci* **35**, 203-225 (2012).
39. Sohal, V.S., Zhang, F., Yizhar, O. & Deisseroth, K. Parvalbumin neurons and gamma rhythms enhance cortical circuit performance. *Nature* **459**, 698-702 (2009).
40. Nase, G., Singer, W., Monyer, H. & Engel, A.K. Features of neuronal

synchrony in mouse visual cortex. *J Neurophysiol* **90**, 1115-1123 (2003).

41. Cho, K.K., *et al.* Gamma rhythms link prefrontal interneuron dysfunction with cognitive inflexibility in Dlx5/6(+/-) mice. *Neuron* **85**, 1332-1343 (2015).
42. Krishnan, G.P., *et al.* Steady state visual evoked potential abnormalities in schizophrenia. *Clin Neurophysiol* **116**, 614-624 (2005).
43. Cho, R.Y., Konecky, R.O. & Carter, C.S. Impairments in frontal cortical gamma synchrony and cognitive control in schizophrenia. *Proc Natl Acad Sci U S A* **103**, 19878-19883 (2006).
44. Minzenberg, M.J., *et al.* Gamma oscillatory power is impaired during cognitive control independent of medication status in first-episode schizophrenia. *Neuropsychopharmacology* **35**, 2590-2599 (2010).
45. Uhlhaas, P.J. & Singer, W. Abnormal neural oscillations and synchrony in schizophrenia. *Nat Rev Neurosci* **11**, 100-113 (2010).
46. Carlen, M., *et al.* A critical role for NMDA receptors in parvalbumin interneurons for gamma rhythm induction and behavior. *Mol Psychiatry* **17**, 537-548 (2012).
47. Billingslea, E.N., *et al.* Parvalbumin cell ablation of NMDA-R1 causes increased resting network excitability with associated social and self-care deficits. *Neuropsychopharmacology* **39**, 1603-1613 (2014).
48. Hellwig, S., *et al.* Altered microglia morphology and higher resilience to stress-induced depression-like behavior in CX3CR1-deficient mice. *Brain Behav Immun* **55**, 126-137 (2016).
49. Rowson, S.A., *et al.* Neuroinflammation and Behavior in HIV-1 Transgenic Rats Exposed to Chronic Adolescent Stress. *Front Psychiatry* **7**, 102 (2016).
50. Wautier, M.P., *et al.* Activation of NADPH oxidase by AGE links oxidant stress to altered gene expression via RAGE. *Am J Physiol Endocrinol Metab* **280**, E685-694 (2001).
51. Toyoshima, M., *et al.* Enhanced carbonyl stress induces irreversible

multimerization of CRMP2 in schizophrenia pathogenesis. *Life Sci Alliance* **2**(2019).

52. Suzuki, R., *et al.* Expression of the receptor for pituitary adenylate cyclase-activating polypeptide (PAC1-R) in reactive astrocytes. *Brain Res Mol Brain Res* **115**, 10-20 (2003).
53. Suzuki, R., *et al.* A transgenic mouse model for the detailed morphological study of astrocytes. *Neurosci Res* **47**, 451-454 (2003).
54. Das, A., *et al.* Hippocampal tissue of patients with refractory temporal lobe epilepsy is associated with astrocyte activation, inflammation, and altered expression of channels and receptors. *Neuroscience* **220**, 237-246 (2012).
55. Mao, D.D., *et al.* Effect of Qingxin Kaiqiao Fang on Hippocampus mRNA Expression of the Inflammation-Related Genes IL-1beta, GFAP, and Abeta in an Alzheimer's Disease Rat Model. *Evid Based Complement Alternat Med* **2018**, 9267653 (2018).
56. Trepanier, M.O., Hopperton, K.E., Mizrahi, R., Mechawar, N. & Bazinet, R.P. Postmortem evidence of cerebral inflammation in schizophrenia: a systematic review. *Mol Psychiatry* **21**, 1009-1026 (2016).
57. Luyendyk, J.P., Schoenecker, J.G. & Flick, M.J. The multifaceted role of fibrinogen in tissue injury and inflammation. *Blood* **133**, 511-520 (2019).
58. Grinberg, L.T. & Thal, D.R. Vascular pathology in the aged human brain. *Acta Neuropathol* **119**, 277-290 (2010).
59. Cortes-Canteli, M., *et al.* Fibrinogen and beta-amyloid association alters thrombosis and fibrinolysis: a possible contributing factor to Alzheimer's disease. *Neuron* **66**, 695-709 (2010).
60. Paul, J., Strickland, S. & Melchor, J.P. Fibrin deposition accelerates neurovascular damage and neuroinflammation in mouse models of Alzheimer's disease. *J Exp Med* **204**, 1999-2008 (2007).
61. Muller, N., *et al.* Celecoxib treatment in an early stage of schizophrenia: results of a randomized, double-blind,

placebo-controlled trial of celecoxib augmentation of amisulpride treatment. *Schizophr Res* **121**, 118-124 (2010).

62. Nitta, M., *et al.* Adjunctive use of nonsteroidal anti-inflammatory drugs for schizophrenia: a meta-analytic investigation of randomized controlled trials. *Schizophr Bull* **39**, 1230-1241 (2013).
63. Thrombosis prevention trial: randomised trial of low-intensity oral anticoagulation with warfarin and low-dose aspirin in the primary prevention of ischaemic heart disease in men at increased risk. The Medical Research Council's General Practice Research Framework. *Lancet* **351**, 233-241 (1998).
64. de Gaetano, G. Low-dose aspirin and vitamin E in people at cardiovascular risk: a randomised trial in general practice. Collaborative Group of the Primary Prevention Project. *Lancet* **357**, 89-95 (2001).
65. Collaborative meta-analysis of randomised trials of antiplatelet therapy for prevention of death, myocardial infarction, and stroke in high risk patients. *Bmj* **324**, 71-86 (2002).
66. Magen, E., *et al.* Effects of low-dose aspirin on blood pressure and endothelial function of treated hypertensive hypercholesterolaemic subjects. *J Hum Hypertens* **19**, 667-673 (2005).
67. Thomas, M.R. & Storey, R.F. The role of platelets in inflammation. *Thromb Haemost* **114**, 449-458 (2015).
68. Jang, C., *et al.* The Small Intestine Converts Dietary Fructose into Glucose and Organic Acids. *Cell Metab* **27**, 351-361.e353 (2018).
69. Schomburg, G.M.a.D. *Biochemical Pathways: An Atlas of Biochemistry and Molecular Biology*, (2012).
70. Hwang, J.J., *et al.* The human brain produces fructose from glucose. *JCI Insight* **2**, e90508 (2017).
71. Sakasai-Sakai, A., Takata, T., Takino, J.I. & Takeuchi, M. Impact of intracellular glyceraldehyde-derived advanced glycation end-products on human hepatocyte cell death. *Sci Rep* **7**, 14282 (2017).
72. Hwang, J.J., *et al.* Fructose levels are markedly elevated in

cerebrospinal fluid compared to plasma in pregnant women. *PLoS One* **10**, e0128582 (2015).

73. Shinozaki, Y.*, et al.* Transformation of Astrocytes to a Neuroprotective Phenotype by Microglia via P2Y1 Receptor Downregulation. *Cell Rep* **19**, 1151-1164 (2017).
74. Tomasella, E.*, et al.* Deletion of dopamine D2 receptors from parvalbumin interneurons in mouse causes schizophrenia-like phenotypes. *Proc Natl Acad Sci U S A* **115**, 3476-3481 (2018).
75. Chen, C.C., Lu, J., Yang, R., Ding, J.B. & Zuo, Y. Selective activation of parvalbumin interneurons prevents stress-induced synapse loss and perceptual defects. *Mol Psychiatry* **23**, 1614-1625 (2018).
76. Lodge, D.J. & Grace, A.A. The hippocampus modulates dopamine neuron responsivity by regulating the intensity of phasic neuron activation. *Neuropsychopharmacology* **31**, 1356-1361 (2006).
77. Lodge, D.J. & Grace, A.A. Aberrant hippocampal activity underlies the dopamine dysregulation in an animal model of schizophrenia. *J Neurosci* **27**, 11424-11430 (2007).
78. Kawaguchi, Y. & Kubota, Y. GABAergic cell subtypes and their synaptic connections in rat frontal cortex. *Cereb Cortex* **7**, 476-486 (1997).
79. Kawaguchi, Y., Katsumaru, H., Kosaka, T., Heizmann, C.W. & Hama, K. Fast spiking cells in rat hippocampus (CA1 region) contain the calcium-binding protein parvalbumin. *Brain Res* **416**, 369-374 (1987).
80. Kann, O. The interneuron energy hypothesis: Implications for brain disease. *Neurobiol Dis* **90**, 75-85 (2016).
81. Buzsaki, G. & Draguhn, A. Neuronal oscillations in cortical networks. *Science* **304**, 1926-1929 (2004).
82. Li, K.J., Greenstein, A.P. & Delisi, L.E. Sudden death in schizophrenia. *Curr Opin Psychiatry* **31**, 169-175 (2018).
83. Koponen, H.*, et al.* Schizophrenia and sudden cardiac death: a review. *Nord J Psychiatry* **62**, 342-345 (2008).
84. Gugliucci, A. Formation of Fructose-Mediated Advanced Glycation

End Products and Their Roles in Metabolic and Inflammatory Diseases. *Adv Nutr* **8**, 54-62 (2017).

85. Chaudhuri, J.*, et al.* The Role of Advanced Glycation End Products in Aging and Metabolic Diseases: Bridging Association and Causality. *Cell Metab* **28**, 337-352 (2018).
86. Menard, C.*, et al.* Social stress induces neurovascular pathology promoting depression. *Nat Neurosci* **20**, 1752-1760 (2017).
87. Banks, W.A.*, et al.* Lipopolysaccharide-induced blood-brain barrier disruption: roles of cyclooxygenase, oxidative stress, neuroinflammation, and elements of the neurovascular unit. *J Neuroinflammation* **12**, 223 (2015).
88. Ben-Nathan, D., Lustig, S. & Danenberg, H.D. Stress-induced neuroinvasiveness of a neurovirulent noninvasive Sindbis virus in cold or isolation subjected mice. *Life Sci* **48**, 1493-1500 (1991).
89. Samuelsson, B., Granstrom, E., Green, K., Hamberg, M. & Hammarstrom, S. Prostaglandins. *Annu Rev Biochem* **44**, 669-695 (1975).
90. Mitchell, J.A., Akarasereenont, P., Thiemermann, C., Flower, R.J. & Vane, J.R. Selectivity of nonsteroidal antiinflammatory drugs as inhibitors of constitutive and inducible cyclooxygenase. *Proc Natl Acad Sci U S A* **90**, 11693-11697 (1993).
91. Schror, K. & Rauch, B.H. Aspirin and lipid mediators in the cardiovascular system. *Prostaglandins Other Lipid Mediat* **121**, 17-23 (2015).
92. Romano, M., Cianci, E., Simiele, F. & Recchiuti, A. Lipoxins and aspirin-triggered lipoxins in resolution of inflammation. *Eur J Pharmacol* **760**, 49-63 (2015).
93. Nascimento-Silva, V., Arruda, M.A., Barja-Fidalgo, C. & Fierro, I.M. Aspirin-triggered lipoxin A4 blocks reactive oxygen species generation in endothelial cells: a novel antioxidative mechanism. *Thromb Haemost* **97**, 88-98 (2007).
94. Dzeshka, M.S., Shantsila, A. & Lip, G.Y. Effects of Aspirin on

Endothelial Function and Hypertension. *Curr Hypertens Rep* **18**, 83 (2016).

95. Hohlfeld, T. & Schror, K. Antiinflammatory effects of aspirin in ACS: relevant to its cardiocoronary actions? *Thromb Haemost* **114**, 469-477 (2015).
96. Hennekens, C.H., *et al.* A randomized trial of aspirin at clinically relevant doses and nitric oxide formation in humans. *J Cardiovasc Pharmacol Ther* **15**, 344-348 (2010).
97. Hetzel, S., *et al.* Aspirin increases nitric oxide formation in chronic stable coronary disease. *J Cardiovasc Pharmacol Ther* **18**, 217-221 (2013).
98. Kalueff, A.V., *et al.* Neurobiology of rodent self-grooming and its value for translational neuroscience. *Nat Rev Neurosci* **17**, 45-59 (2016).
99. Jirkof, P. Burrowing and nest building behavior as indicators of well-being in mice. *J Neurosci Methods* **234**, 139-146 (2014).
100. Pedersen, C.S., Sorensen, D.B., Parachikova, A.I. & Plath, N. PCP-induced deficits in murine nest building activity: employment of an ethological rodent behavior to mimic negative-like symptoms of schizophrenia. *Behav Brain Res* **273**, 63-72 (2014).
101. Forsingdal, A., Fejgin, K., Nielsen, V., Werge, T. & Nielsen, J. 15q13.3 homozygous knockout mouse model display epilepsy-, autism- and schizophrenia-related phenotypes. *Transl Psychiatry* **6**, e860 (2016).
102. Ennaceur, A. & Delacour, J. A new one-trial test for neurobiological studies of memory in rats. 1: Behavioral data. *Behav Brain Res* **31**, 47-59 (1988).
103. Tellez, L.A., *et al.* Separate circuitries encode the hedonic and nutritional values of sugar. *Nat Neurosci* **19**, 465-470 (2016).
104. Golde, W.T., Gollobin, P. & Rodriguez, L.L. A rapid, simple, and humane method for submandibular bleeding of mice using a lancet. *Lab Anim (NY)* **34**, 39-43 (2005).

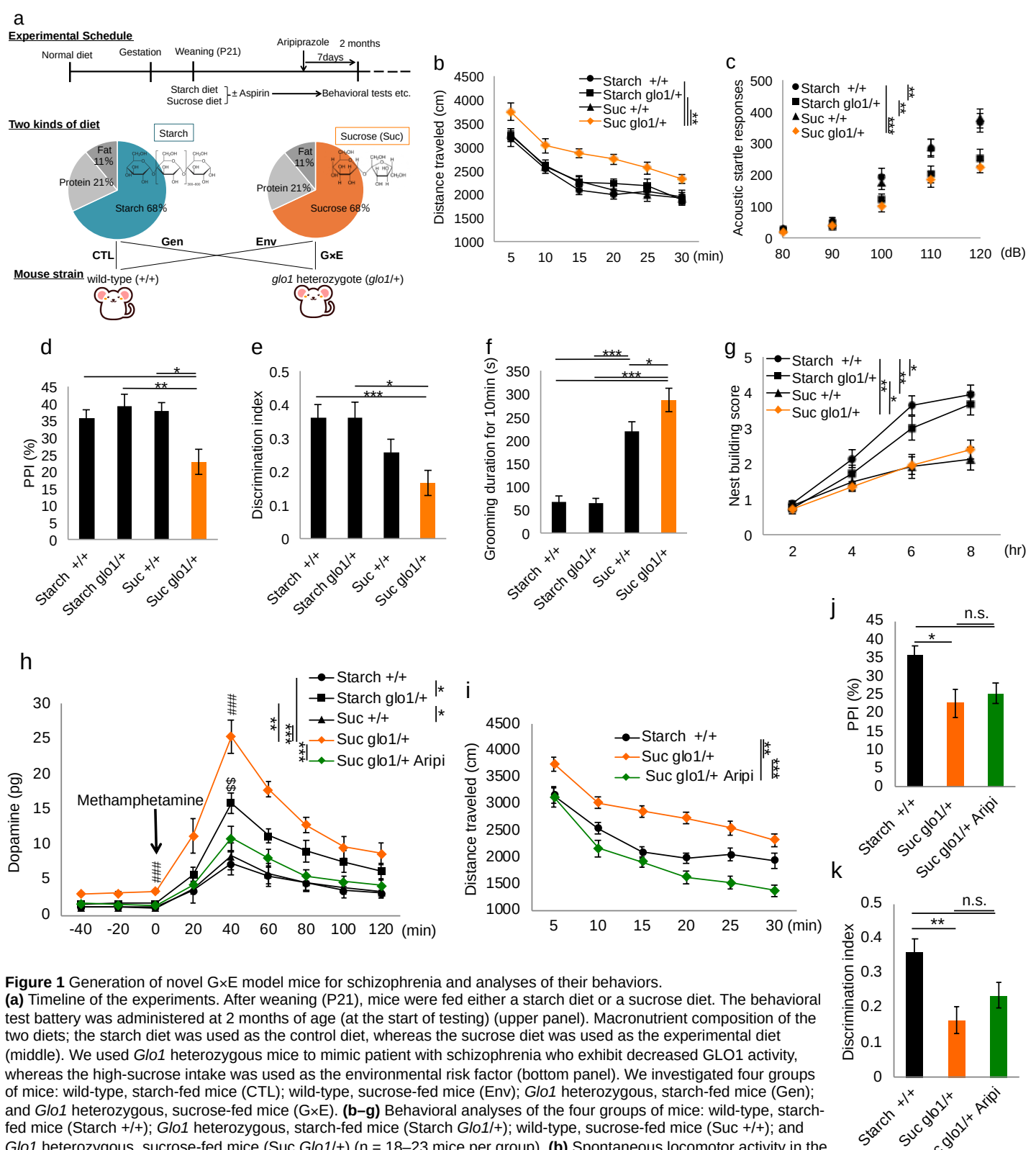

Figure 1 Generation of novel G×E model mice for schizophrenia and analyses of their behaviors.
(a) Timeline of the experiments. After weaning (P21), mice were fed either a starch diet or a sucrose diet. The behavioral test battery was administered at 2 months of age (at the start of testing) (upper panel). Macronutrient composition of the two diets; the starch diet was used as the control diet, whereas the sucrose diet was used as the experimental diet (middle). We used *Glo1* heterozygous mice to mimic patient with schizophrenia who exhibit decreased GLO1 activity, whereas the high-sucrose intake was used as the environmental risk factor (bottom panel). We investigated four groups of mice: wild-type, starch-fed mice (CTL); wild-type, sucrose-fed mice (Env); *Glo1* heterozygous, starch-fed mice (Gen); and *Glo1* heterozygous, sucrose-fed mice (G×E). **(b–g)** Behavioral analyses of the four groups of mice: wild-type, starch-fed mice (Starch +/+); *Glo1* heterozygous, starch-fed mice (Starch *Glo1*/+); wild-type, sucrose-fed mice (Suc +/+); and *Glo1* heterozygous, sucrose-fed mice (Suc *Glo1*/+) (n = 18–23 mice per group). **(b)** Spontaneous locomotor activity in the open-field test. **(c)** Acoustic startle responses. **(d)** Pre-pulse inhibition for the 70 dB pre-pulse sound levels. **(e)** Object-location test (to evaluate working memory over 5 min). **(f)** Duration of self-grooming in the home cage. **(g)** Quantification of nest-building skills over 8 h. **(h)** Extracellular concentration of dopamine in the nucleus accumbens, as measured at 20-min intervals using an *in vivo* microdialysis system. Methamphetamine (1.25 mg/kg) was administered i.p. at time 0 (arrow) (n = 8–11 mice per group). **(i–k)** Effects of aripiprazole (Aripi) treatment on abnormal behaviors (n = 16–18 mice per group). **(i)** Quantifications of locomotor activity. **(j)** PPI for the 70 dB pre-pulse sound levels. **(k)** Object-location test. The statistical tests used included the Tukey–Kramer test **(d, e, f, j, and k)** and two-way repeated-measures ANOVA **(b,c,g,h, and i)**; the main effect of group in **b** (F3, 73 = 6.19, $P = 0.0008$), **c** (F3, 63 = 6.75, $P = 0.0005$), **g** (F3, 81 = 6.67, $P = 0.0004$), **h** (F4, 36 = 14.0374), and **i** (F2, 51 = 27.59, $P < 0.0001$) was followed by Shaffer's multiple comparisons test of genotype groups. **(h)** Bonferroni multiple comparisons test of genotype groups at specific time points, ###$P < 0.001$ for Suc *Glo1*/+ vs. Ctrl (Starch +/+), $$$P < 0.01$ for Starch *Glo1*/+ vs. Ctrl (Starch +/+). Data are means ± s.e.m. *$P < 0.05$, **$P < 0.01$, ***$P < 0.001$; n.s., not significant.

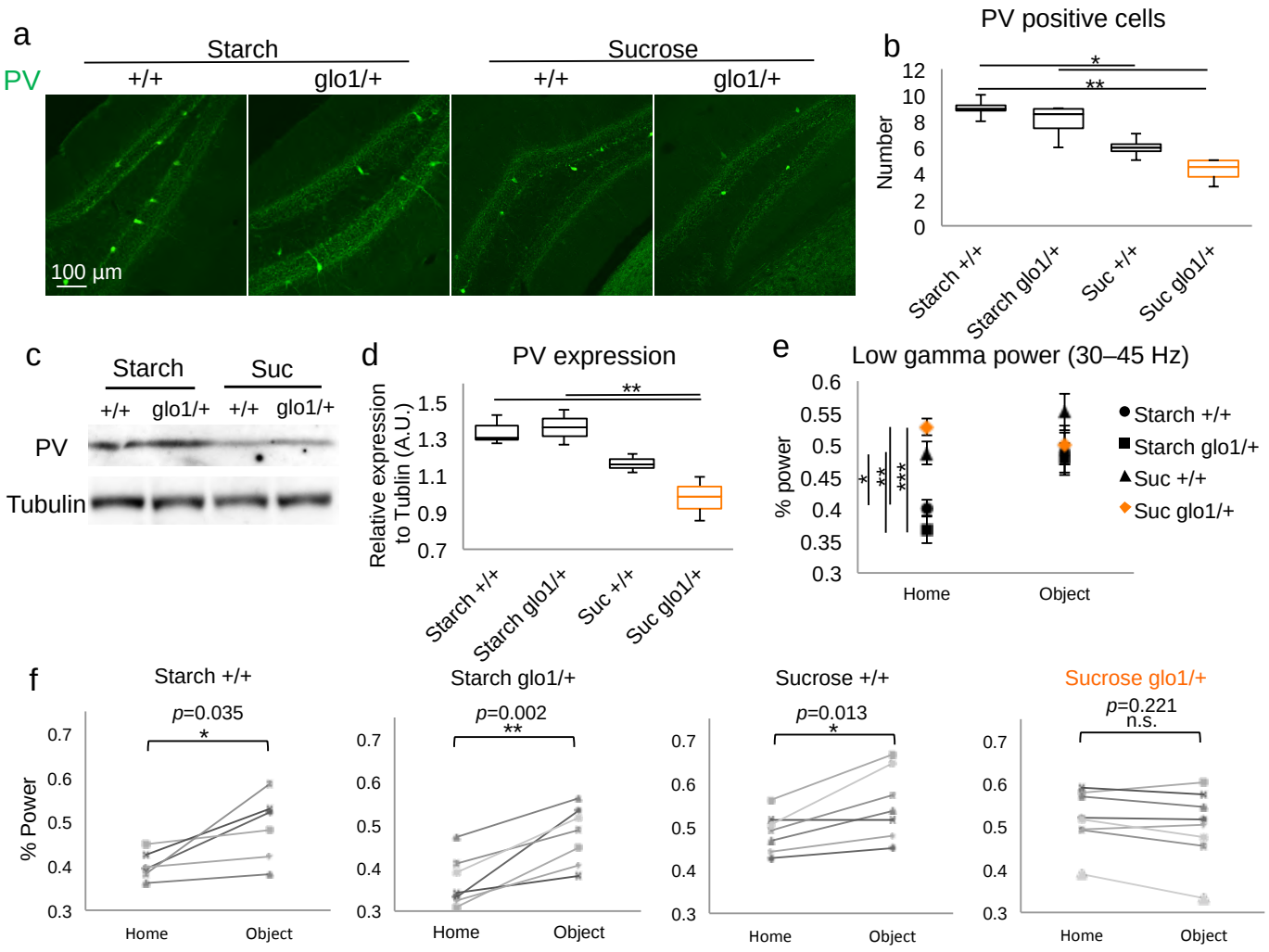

Figure 2 Parvalbumin-positive interneuron dysfunction in G×E mice.
(a) Immunohistochemistry of parvalbumin (PV) in the hippocampal dentate gyrus (DG). **(b)** Number of PV-positive cells in the DG in a (n = 4 slices per group). **(c)** Western blot analysis of the PV protein using tubulin as the internal control. **(d)** Densitometric analysis of the expression levels of the PV protein in c. To evaluate the expression levels of PV, the intensities of the bands in c were divided by their corresponding intensities in the control (tubulin) (n = 3 mice per group). **(e)** Average gamma band power in the home cage and novel object recognition phase (n = 7–8 mice per group). **(f)** Changes in gamma band power from the home cage to the novel object observed in individual mice (n = 7–8 mice per group). The statistical tests used included the Tukey–Kramer test **(b,d, and e)** and two-way repeated-measures ANOVA **(f)**; the main effect of group in **b** (F3, 73 = 6.19, *P* = 0.0008), **c** (F3, 63 = 6.75, *P* = 0.0005), **g** (F3, 81 = 6.67, *P* = 0.0004), **h** (F4, 36 = 14.0374), and **i** (F2, 51 = 27.59, *P* < 0.0001) was followed by Shaffer's multiple comparison test of genotype groups.

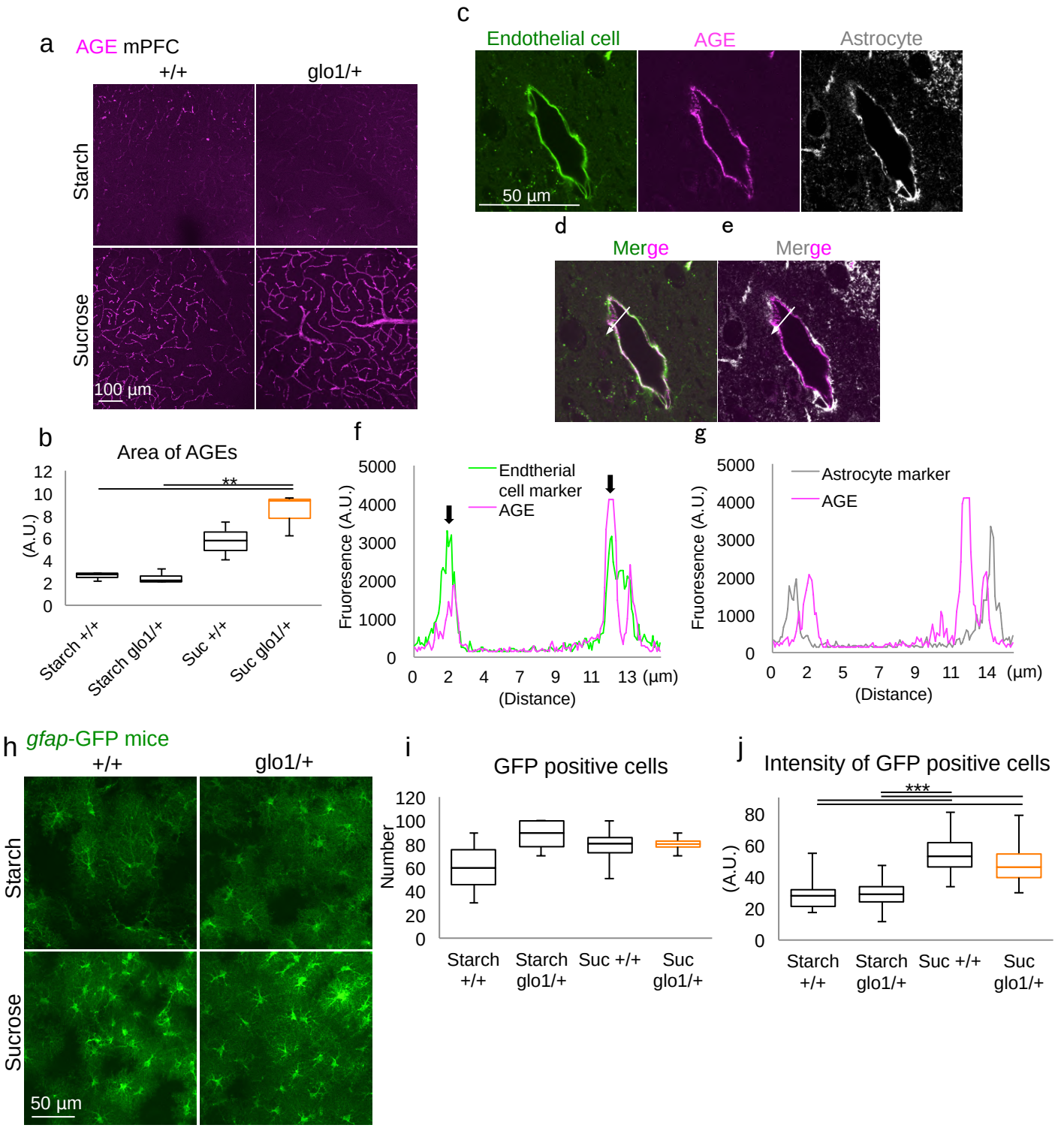

Figure 3 AGE accumulation and pre-inflammatory status of astrocytes in G×E mice.
(a) Images of the results of immunohistochemistry for AGEs in the medial prefrontal cortices. **(b)** Measurement of the area covered by AGEs in a, where the area is above the appropriate threshold of pixel intensity in each image (n = 3 slices per group). The mean intensity of the entire image was measured in each section. **(c–e)** Immunohistochemical data including images of colocalization between tomato-lectin (endothelial cell marker) or Aldh1l1 (astrocyte marker) and AGEs. **(f,g)** Plots of pixel intensities along the white arrow in d for f, and e for g. The black arrows in f indicate colocalization points of lectin and AGEs. **(h)** Immunohistological images of GFP-positive astrocytes in the hippocampal CA1 region. **(i)** Number of GFP-positive cells in each image presented in h. No significant differences were observed among the groups. **(k)** Mean fluorescent intensities of 10 randomly selected cells per image from the hippocampal CA1 region of four independent mice. The statistical tests used included the Tukey–Kramer test in **b**,**i**, and **j**. $^{**}P < 0.01$; $^{***}P < 0.001$.

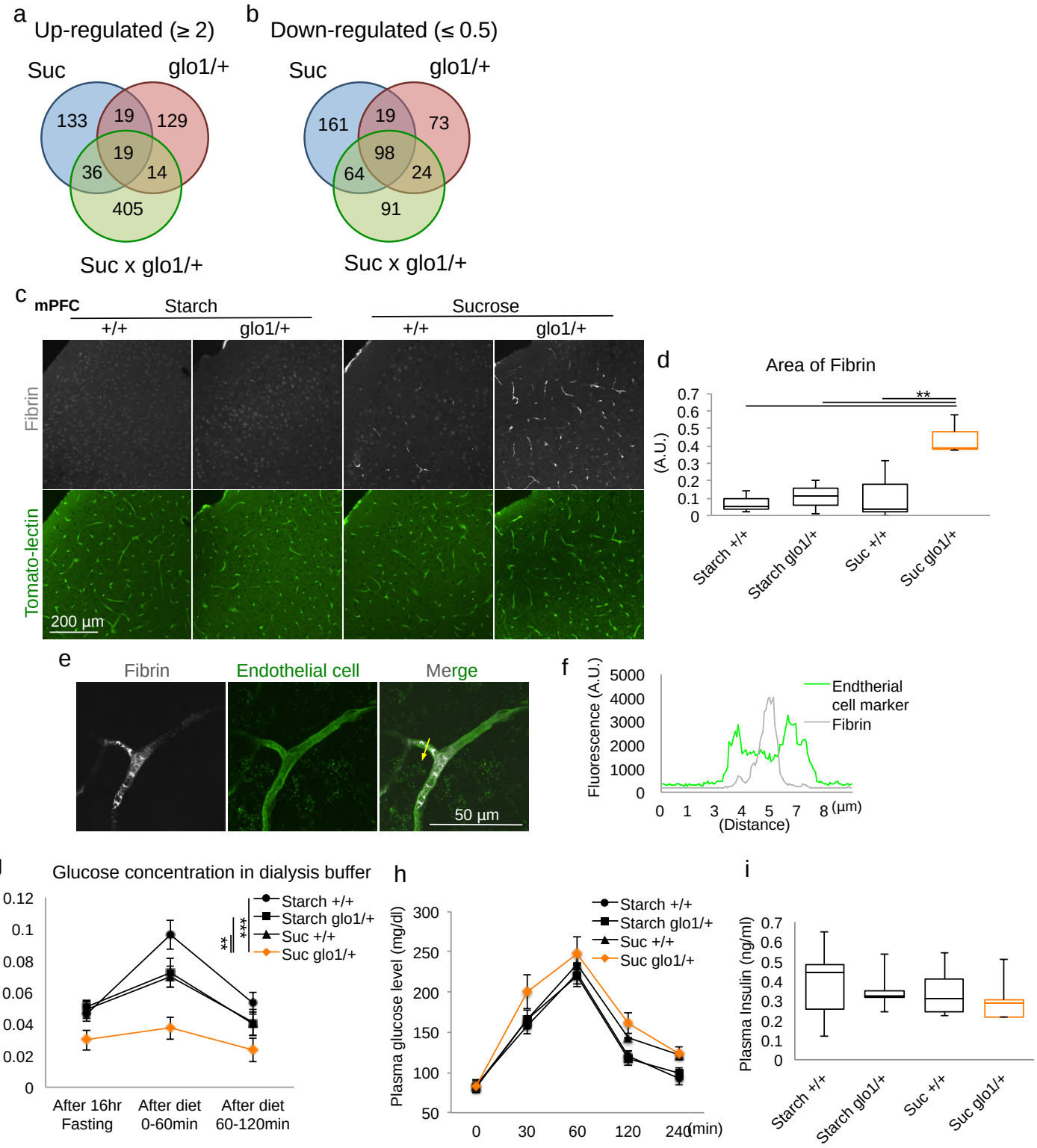

Figure 4 Angiopathy and impaired glucose incorporation observed in G×E mice.
(a,b) Venn graph showing the overlap in the genes that exhibited >2-fold **(a)** or <0.5-fold **(b)** expression levels compared with the CTL group using PFC samples (n = 3 per group). **(c)** Immunohistochemical images of fibrin and the endothelial cell marker tomato-lectin. **(d)** Measurement of the area covered with fibrin in c, where the area is above the appropriate threshold of pixel intensity in each image (n = 3 slices per group). The mean intensity of the entire image was measured for each section. **(e)** Co-immunohistochemical images of tomato-lectin with fibrin in the medial prefrontal cortices. **(f)** Plots of pixel intensities along the yellow arrow in e. **(g)** Extracellular concentrations of glucose in the dialysis buffer at each time point (1 h collection after 16 h of fasting; for 1 h after eating a 0.05 g diet; for 1 h from 1 h after eating a 0.05 g diet) (n = 5–6 mice per group). **(h)** Plasma glucose levels in wild-type and *Glo1* heterozygous mice (n = 6–7 mice per group). The first measurement was performed after 16 h of fasting, and the second blood collection was performed 30 min after eating a 0.05 g diet. No significant differences were observed among the groups. **(i)** Fasting plasma insulin levels in wild-type and *Glo1* heterozygous mice. No significant differences were observed between the groups (n = 5–6 mice per group). Further, the 0.05 g diet we used in g, h, and i were daily eaten by mice in each group (0.05 g sucrose for the daily sucrose eating group and 0.05 g starch for the daily starch eating group). The statistical tests used included two-way repeated-measures ANOVA in **g** and **h**; main effect of group in **g** ($F3, 23 = 5.7851$, $P = 0.0042$) and **h** ($F3, 23 = 2.9734$, $P = 0.0528$), and the Tukey–Kramer test in **d** and **i**. The data are presented as the mean ± s.e.m. $^{**}P < 0.01$; $^{*}P < 0.05$.

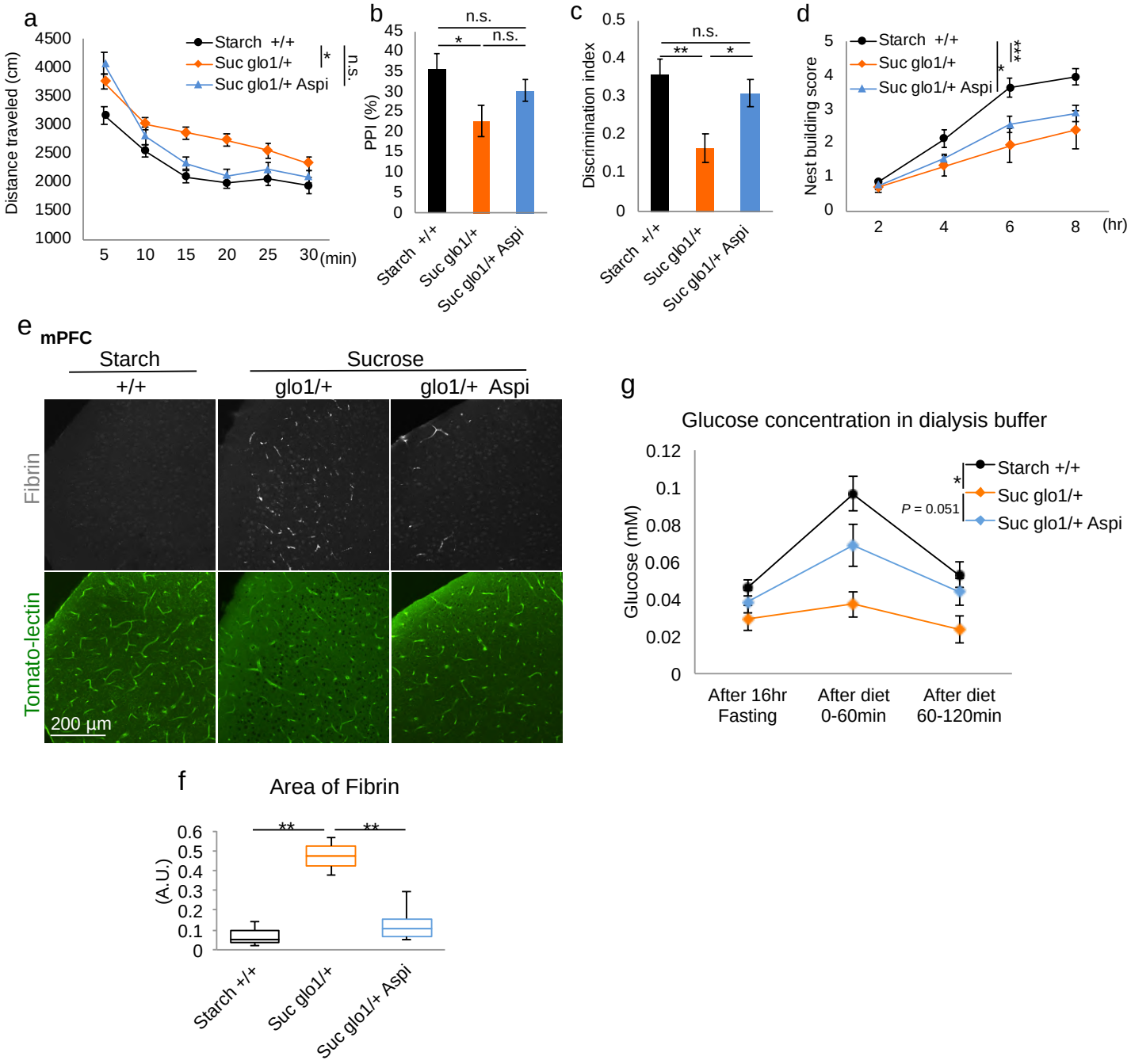

Figure 5 Protective effects of low-dose aspirin against the impairments observed in G×E mice.
(a–d) Results of behavioral tests that were performed to evaluate the effects of aspirin treatment (n = 12–21 mice per group). **(a)** Quantifications of spontaneous locomotor activity using the open-field test. **(b)** Pre-pulse inhibition test at 70 dB. **(c)** Object-location test (to evaluate working memory over 5 min). **(d)** Quantification of nest-building skills over 8 h (n = 12–21 mice per group). **(e)** Immunohistochemical images of fibrin and the endothelial cell marker tomato-lectin. **(f)** Measurement of the area covered with fibrin in **e**, in which the area is above the appropriate threshold of pixel intensity in each image (n = 3 slices per group). The mean intensity of the entire image was measured for each section. **(g)** Extracellular concentrations of glucose in the dialysis buffer at each time point (1 h collection after 16 h of fasting, for 1 h after eating a 0.05 g diet, for 1 h from 1 h after eating a 0.05g diet) (n = 4–6 mice per group). The statistical tests used included the Tukey–Kramer test in **b**, **c**, and **f**; two-way repeated-measures ANOVA in **a** and **d**; main effect of group in **a** ($F_{2, 50} = 6.4385$, $P = 0.0033$), **d** ($F_{2, 49} = 8.0315$, $P = 0.001$) and **g** ($F_{2, 17} = 6.1758$, $P = 0.0096$). The data are presented as the mean ± s.e.m. *$P < 0.05$; **$P < 0.01$; ***$P < 0.01$.

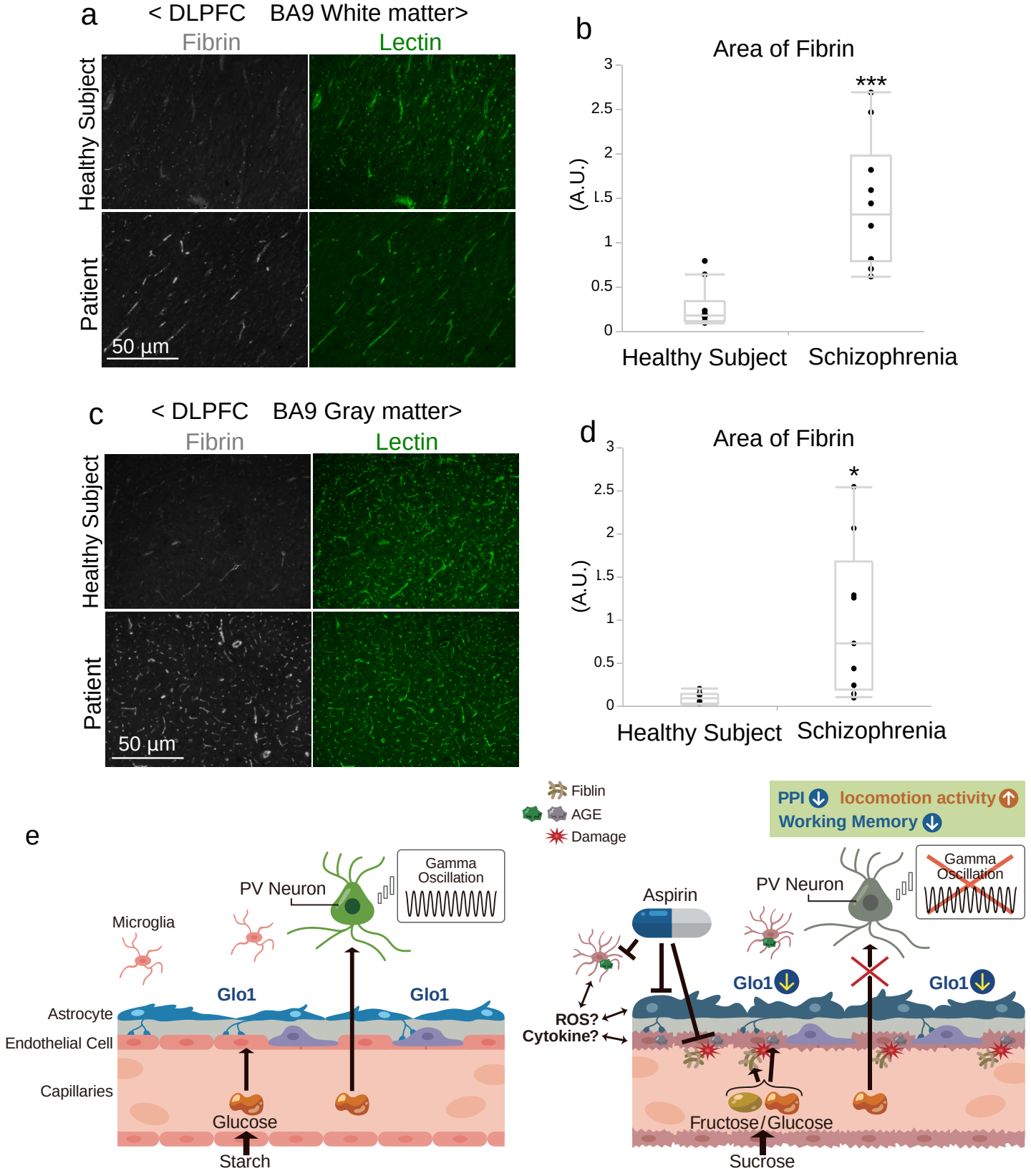

Figure 6 Vascular injury in postmortem brains from individuals with schizophrenia.
(a, c) Representative immunohistochemical images of fibrin (gray) and the endothelial cell marker tomato-lectin (green) in postmortem brains from healthy controls and patients with schizophrenia: white matter **(a)** and gray matter **(c)**. **(b, d)** Measurement of the area covered with fibrin in **a** and **c**, in which the area is above the appropriate threshold of pixel intensity in each image (n = 10 slices per group). The mean intensity of the entire image was measured for each section. The statistical tests used included the Tukey–Kramer test in **b** and **d**. The data are presented as the mean ± s.e.m. *$P < 0.05$; ***$P < 0.01$. **(e)** Diagrams describing the hypothesis that was proposed to explain the phenomena observed in CTL mice (left) and in G×E mice (right). (see the Discussion section for details).